（千葉大学審査学位論文）

Adsorption of Biological Materials on Porous Solids: Mechanism and Medical Application

（細孔性固体と生体物質の相互作用の解明と

その生物工学的応用）

2015 年 1 月

千葉大学大学院理学研究科

基盤理学専攻化学コース

井上　覚

Contents

Abstract

Porous materials have been used in many industrial fields as adsorbent, catalysis carrier, separation materials and so on. Activated carbons (ACs) is the most popular porous material as adsorbent for purification fields and medical field because of high pore volume and surface area. The most signalized character of ACs is its high no specified adsorption ability. As for medical usage, ACs historically was used for treatment of poisoning as oral medicine and extracorporeal blood therapy adsorbent.

The adsorption ability depends on their pore structure. Thus, characterization of porous materials is essential for their applications. For medical usage, mesopore and macropore is suitable for biological materials; protein, prokaryote, adsorption because of their pore size.

In this thesis, gas adsorption mechanism on mesopore were examined and analyzed. Saam-Cole approach, which is added the surface-molecular interactions in mesopore to Kelvin approach, was introduced to N_2, He, and O_2 adsorption measurements on various pore size mesoporous silica (2.5 nm-4.1 nm) and two kinds of carbon aerogel and discuss the cause of adsorption hysteresis existence both theoretically and experimentally.

Recently in medical fields, the extracorporeal adsorbent for adsorbing cytokines and alarmin for treatment of sepsis and systemic inflammatory response syndrome (SIRS) have been investigated. The adsorbent is required to adsorb not only specific cytokine but also adsorb cytokines exhaustively. Because inflammatory conditions and multiple organ failure due to sepsis and SIRS result from the excessive immune response of many type of cytokines and alarmins. Thus, the investigation of the ability of ACs to simultaneously adsorb many different cytokines is important to determine whether ACs is effective adsorbent for the suppression of sepsis and SIRS.

In this thesis, the ability of an ACs to adsorb 18 different cytokines with molecular weights

ranging from 8 kDa to 70 kDa and high mobility group box 1 (HMGB1) from inflammatory model plasma at 310 K and the mechanisms of adsorption were examined. Porosity analysis using N_2 gas adsorption at 77 K showed that the AC had micropores with diameter of 1-2 nm and mesopores with diameter of 5-20 nm. All 18 cytokines and HMGB1 were adsorbed on the ACs; however, the shapes of the adsorption isotherms changed depending on the cytokine molecular weight. The adsorption isotherms for molecules of 8-10 kDa, 10-20 kDa, 20-30 kDa, and higher molecular weights were classified H-2, L-3, S-3 and S-1 types, respectively. These results suggested that the adsorption mechanism for the cytokines and HMGB1 in the mesopore and on the surface of the AC differed as a function of the molecular weight. On the basis of these results, it can be concluded that AC should be efficient for cytokine adsorption.

In this thesis, we also examined the efficacy of porous material for removing the pathogen of infectious disease; Chagas disease. Chagas disease is the infectious disease caused by *T. cruzi* which is the prokaryote (1-5 μm). The removal ability of *T. cruzi* by cellulose porous beads (CPB) from infectious model blood was examined. Porosity analysis using mercury porosimeter showed that CPB had macropores with pore width about 10 μm. By flowing infectious model blood in the CPB column, the concentration of *T. cruzi* decreased about one-hundredth. According to the analysis of surface of CPB after flowing experiment, *T. cruzi* adhered on the surface of CPB. From this analysis and the mechanism of *T. cruzi* cell penetration, we estimated that the chemical structure of CPB surface is resembled to the chemical structure of *T. cruzi* recognition part when *T. cruzi* invade in cells.

1. General Introduction

Porous materials with large pore volume and surface area have been utilized in various industrial fields as medicine, medical adsorbent, catalyst carrier, electric devices, and so on. For these applications, various porous materials have been developed. In order to utilize for many industrial fields, there have been developed many kinds of porous materials. The functions of porous materials depend on their porosity; pore volume, surface area and so on.

Activated Carbons (ACs) have long history of many industrial applications; water and air purification, medical adsorbent for oral use. These applications were because of its powerful non-specific adsorption capacities (1). ACs have been widely used in medicine since ancient times for the treatment of food poising. In 1900s, activation processes were developed to great increase the adsorption capacity of derived carbons and useful resources for pyrolysis were better defined for a more superior products. From this period, ACs were also used for the treatment of poisoning and drug overdose (2, 3). From middle of 1900s, ACs also started to use as adsrobent for hemoperfusion. Hemoperfusion is the medical treatments to remove drug and poison from blood and plasma by exrtacopreal treatments. In these days, ACs just used as adsorbent for removal small range molecules by oral and extracopreal treatments (4).

In early 1990s, there have been developed the technique for synthesising the highly uniform porous materials by molecular template method and started to make uniform mesoporous silicate; FSM, MCM (5, 6). These uniform mesoporous materials used for cathodes of Li-ion battery and catalyst carrier. These uniform mesoporous materials also presented the curious phenomenon. Conventionally, the adsorption isohterms of mesoporous materials showed adsorption hysterisis. But some of the these uniform mesoporous materials did not show adsorption hysterisis. It have not been clear the reason why adsorption hysterisis was disappeared.

In 1991, helical microtube of graphite was discovered and start to resarch for its properties and production method (7). In this two decade, there have been developed many kinds of porous material and can control their pore width frexibly.

At the same days, extracoporeal techniqe was progressivly developed and popularized. It became clear that important mediators of sepsis and systemic inflammatory syndrom (SIRS) were cytokines and alarmins, which is middle molecular protein. The needs for removeing cytokines and alarmins rase in this period. However conventional ACs for poisonig treatment can't adsorb large molecules because of their porosities. The pore width of ACs is too small to adsorb middle range protein molecules like cytokines and alarmins. After 2000, condition of activation started to examine and can meke ACs which have mesoporo. These mesoporous ACs started to evaluated their certain kinds of cytokines (8-12).

Sepsis and SIRS were mainly caused by infection of Grum negative bacteria and developed by many kinds of cytokines and alarmins networks (13). Therefore today's evaluation of cytokine adsorbent for sepsis and SIRS treatment were not enough to evaluate ACs fesibility for sepsis and SIRS treatments. In addition to this, the mechanisms of cytokines and alarmins adsorption still unknown.

In a medical field, in addition to cytokine removals, there are many expectation to blood purification. Pathogen removal of infectious disease is one of the expectation for blood purification by porous materials. The parasite removal by using large mesoporous and macroporous materials have been examined.

In this doctroral thesis, I forcused on the relation between porosities and many kinds cytokines and alarmins adsorption ability of ACs for evaluating the feasibility as sepsis and SIRS treatment adsorbent. And I also declared cytokines and alarmin adsorption mechanism on ACs in Chapter 3-1.

The feasibility of large mesoporous and macroporous cellulose beads (CPB) as the parasite adsorbent from blood were examined. This doctroral thesis forcused on the pathogen of Chagas disease; *T. cruzi*, which is the local infectious disease in Latein America. I discussed the porosities of CPB and T. cruzi adsorption in Chapter 3-2.

Before discussing the porosity and utilization of porous materials for medical adsorbents, I make reference to the fandamentals of gas and liquid adsorption on porous materials and characterization of porous materials. Especially, I examined gas adsorption on mesoporous materials which have various different uniform pore width and analyzed the mechanism of gas adsorption and disappearance of hysterisis by introducing Saam-Cole approach in Chapter 2.

References

Chapter 1

(1) S.V. Mikhalovsky, Novel Carbon Adsorbents, Chapter 21, Elsevier, 2012, http://dx.doi: 10.1016/13978-0-08-097744-7.00021-1.

(2) D.O. Cooney, Activated Charcoal in Medical Applications. Marcel Dekker Inc. New York, 1995, http://dx.doi: 10.1201/b14201.

(3) B.G. Katona, E.G. Siegel, R.J. Cluxton Jr., The new black magic: activated charcoal and new therapeutic uses. J Emerg Med, 5, 1987, 9-18, http://dx.doi: 10.1016/0736-4679(87)90004-7.

(4) E. Denti, J.M. Walker, Activated Carbon; properties, selection and evaluation, in C. Giordano (Ed.) Sorbent and their Medical application. Academic Press, New York.1980, ISBN: 978-0-122-85250-3

(5) S. Inagaki, Y. Fukushima, K. Kuroda, Synthesis of highly ordered mesoporous materials from layered polysilicate. J Chem. Soc. Chem. commun. 8, 1993, 680, http://dx.doi: 10.1029/c39930000680.

(6) C.T. Kresge, M.E. Leonowicz, W.J. Roth, J.C. Vartuli, J.S. Beck, Ordered mesoporous molecular sieves synthesized by liquid-crystal template mechanism. 359, 1992, 710-712, http://dx.doi: 10.1038/359710a0.

(7) S. Iijima, Helical micro tubes of graphitic carbon. Nature 354, 1992, 56-68, http://dx.doi: 10.1038/354056a0.

(8) D.J. Malik, G.L. Warwick, M. Venturi, M. Streat, K. Hellgardt, N. Hoenich, J.A. Dale, Preparation of novel mesoporous carbons for the adsorption of an inflammatory cytokine(IL-1β). 25, 2004, 2933-2940, http://dx.doi: 10.1016/j.biomaterials.2003.09.076.

(9) C.A. Howell, S.R. Sandeman, G.J. Philips, A.W. Lloyd, J.G. Davies, S.V. Mikhalovsky, S.R.

Tennison, A.P. Rawlinson, O.P. Kozynchenko, H.L.H. Owen, J.D.S. Gaylor, J.J. Rouse, J.M.Courtney, The in vitro adsorption of cytokines by polymer-pryrolysed carbon. 27, 2006, 5286-5291, http://dx.doi: 10.1016/j.biomaterials.2006.05041.

(10) G. Yushin, E.N. Hoffman, M.W. Barsoum, Y.Gogotsi, C.A Howell, S.R. Sandeman, G.J. Philips, A.W. Lloyd, S.V. Mikhalovsky, Mesoporous carbide-derived carbon with porosity tuned for efficient adsorption of cytokines. 27, 2006, 5755-5762, http://dx.doi: 10.1016/j.biomaterials.2006.07.019.

(11) S. Yachamaneni, G. Yushin, S.H. Yean, Y. Gogotsi, C. Howell, S. Sandeman, G. Philips, S. Mikhalovsky, Mesoporous carbide-derived carbon for cytokine removal from blood plasma. 31, 2010, 4789-4794, http://dx.doi: 10.1016/j.biomaterials.2010.02.054.

(12) C.A. Howell, S.R. Sandeman, G.J. Philips, S.V. Mikhalovsky, S.R. Tennison, A.P. Rawlinson, O.P. Kozyncheko, Nanoporous activated carbon beads and monolithic columns as effective hemoadsorbents for inflammatory cytokines. Int J Artif Organs 36, 2013, 624-632, http://dx.doi: 10.5301/ijao.5000231.

(13) H. Wang, S. Na, The cytokine storm and factors determining the sequence and severity of organ dysfunction in multiple organ dysfunction syndromes. Am J Emerg Med, 26, 2008, 711-715, http://dx.doi: 10.1016/j.ajem.2007.10.031.

2. Fundamentals of Adsorption

2-1. Introduction

Adsorption phenomena have been utilized in many industrial fields and daily life; water and gas purification, medicinal field, medical field. These adsorption phenomena are one of the most important phenomena for today's industry and daily life. Therefore, many researches have been developed for many years.

One of the most popular materials for adsorbent is activated carbon (AC) which has many pores on its surface and has high surface area. Their application in water purification can be dated back to the era of ancient Egyptians. The major development of adsorbent began during World War II, when activated carbon was manufactured for use in gas masks.

'Adsorption phenomena' is defined the high concentrated material state near the interface between solid-gas, liquid-solid and so on, without chemical reaction.

The materials which adsorbed on the interface are called 'adsorbate'. The materials which make interface are called 'adsorbent'. Concentration of adsorbate molecules is high on the surface of adsorbent. This phenomenon called 'Adsorption phenomena'.

Adsorption phenomena are caused by interaction force between adsorbate and adsorbent; dispersion force, electric force (dipole-dipole interaction, elect quadropole interaction, electrostatic interaction and so on), hydrogen bond and chemical reaction.

The properties of surface electrostatic, hydrophobicity, hydrophilicity have influence on adsorption phenomena. In addition to these surface properties, it also have been known that the structure of surface influence on adsorption phenomena. Especially porous structure on surface has a great influence on adsorption. Interaction force between adsorbate and porous material surface is dispersion force.

Dispersion force interaction between surface and adsorbate is caused by the polarization of adsorbate molecule. This polarization of molecule induces weak electrostatic interactions between adsobate molecules and surface. These adsorption caused by dispersion force called 'physical adsorption'.

Dispersion force interaction is deeply connected with the potential energy of the surface. Small potential energy means stable condition.

The potential energy of surface by dispersion force is expressed by the following equation (2-1) (1).

$$U(r) = -\frac{a}{r^6} + \frac{b}{r^{12}} \qquad (2\text{-}1)$$

where

U(r) = potential energy, r: the distance of adsorbed molecule from the surface, a, b: characteristic attraction and repulsion constants for adsorption systems; gas-solid, liquid-solid systems.

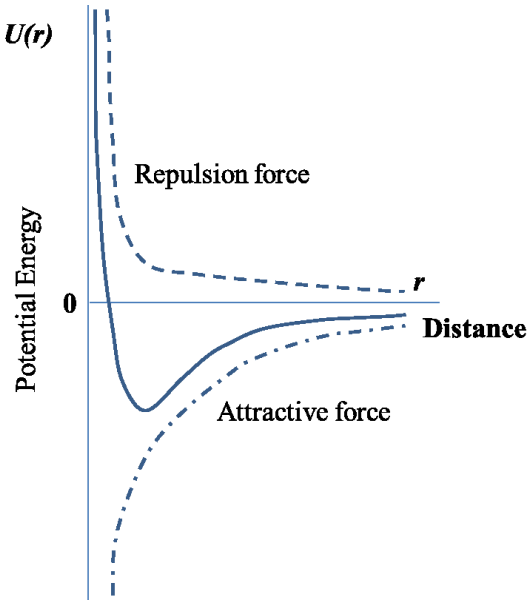

Fig.2-1-a; Potential energy

The r^{-6} and r^{-12} terms in equation 2-1 are associated with the short-range dispersion attractive and repulsion forces respectively, which always contribute to adsorb and are therefore known as the non-specific interactions (2). Fig.2-1-a shows the relation between adsorbate-surface distance and potential energy. Fig.2-1-a indicated that the interaction energy become minimum value at the certain distance from surface. Therefore adsorbate will be concentrated at certain distance from the surface. This is the mechanism of physical adsorption.

Fig.2-1-b shows the potential energy of the two confronted surface. Each surface has potential energy profile like Fig.2-1-a. Fig.2-1-b shows the potential energy profile which is synthesized each potential energy profile. Fig.2-1-b indicates that the minimum energy of two confronted surface system is lower (more stable) than that of single surface. This confronted surface system is just called a pore. Therefore the surface of porous materials is more stable than that of normal surface. Fig.2-1-c shows the interaction energy of narrower pore system. The minimum potential energy is lower than that of wider pore and normal surface.

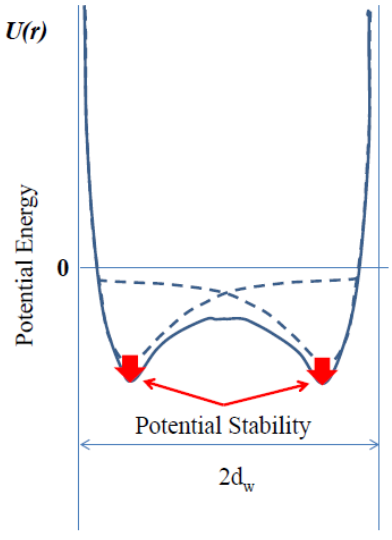

Fig.2-1-b; Wider pore potential stability

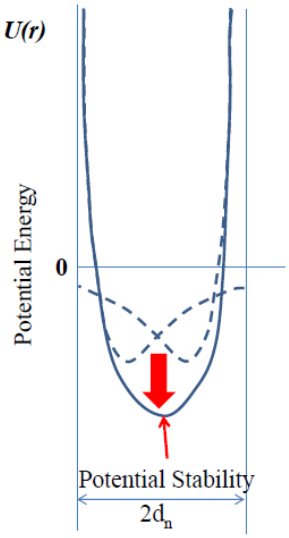

Fig.2-1-c; Narrower pore potential stability

According to the dispersion force potential analysis, the narrower the distance between surfaces is, the more the potential energy become stable to adsorb. Porous materials; e.g. activated carbons, are known as excellent adsorbent materials.

The adsorbed ability of porous materials depends on their pore structure, especially their pore width. The pore width is one of the important factors to characterize porous materials. Porous materials are classified by their pore width (w). IUPAC classifies porosities as follows (3).

Micropore $w < 2.0$ nm

(Ultramicropore $w < 0.7$ nm)

Mesopore $2.0 \text{ nm} < w < 50$ nm

Macropore $w > 50$ nm

It has also been useful to classify micropore further into ultra- (< 0.7 nm width), this definition being relevant when considering adsorption behavior. Micropores are considered as being about the size of adsobate molecules and accommodate one, two or more molecules. Mesoporosity is wider and is characterized by hysteresis loops during adsorption and desorption at high relative pressure of adsorption. Macroporosity has little interest for surface research. They are transport pores to the interior of particles and are considered as external surface.

This doctoral thesis discussed the porosities and medical application of porous materials and adsorption mechanism. Therefore in this chapter, I refer the fundamentals of gas-solid adsorption as a method for porous materials characterization and liquid-solid adsorption for analyzing the cytokine and HMGB1 adsorption from plasma and pathogen of Chagas disease from blood.

2-2.Gas Adsorption as a Method for Characterization of Porous Materials

Characterization of Adsorption Isotherms and Pore Structure

Porous materials are characterized by many methods; gas adsorption, microcalorimetry, small angle scattering of X-rays (SAXS), transmission electron microscopy, mercury porosimeter and so on. Gas adsorption is one of the most widely used methods for the characterization of non-crystalline porous materials like activated carbons. The aim of most routine work to determine the surface area, pore width, pore volume, pore size distribution but this is not always easy to achieve. The complexity of both the pore structure and mechanisms of adsorption makes it necessary to adopt a cautious approach in the interpretation of experimental data. On the other hand, adsorption measurements provide useful information of microstructure and are essential if the porous material is to be used as an adsorbent.

In this chapter, I refer how to take pore structure information from gas adsorption measurement.

Adsorption Isotherms

The amount adsorbed, n, by unit mass of solid (adsorbent) is dependent on the gas (adsorbate) pressure, p, the temperature, T, the properties of the adsorbent and nature of gas-solid interactions. Thus, for the adsorption of given adsorbate by particular adsorbent, we may write the following equation (2-2),

$$n = f(p,T)_{system} \qquad (2\text{-}2)$$

and at constant temperature.

$$n = f(p)_{T,system} \qquad (2\text{-}3)$$

Equation (2-3) represents the adsorption isotherm, which is generally presented in the graphical form of n plotted against p or p/p_0, where p_0 is the saturation pressure of the adsorbate at the temperature of the measurements.

Adsorption isotherms are studied to obtain information as follows.

- estimation of surface area
- estimation of pore volume in the various porosities presents; pore-width, potential energy of pores
- estimation of the surface chemistry of the adsorbent; hydrophobicity, hydrophilicity
- estimation of adsorption process, i.e. the properties of adsorption phase

The interpretation of adsorption isotherms is not provided direct information of pore structure. We need to analyze the adsorption isotherms by various ways.

I would like to inform the method to analyze the adsorption isotherms for understanding pore structure of adsorbent and adsorption mechanism in following sections.

Classification of Adsorption Isotherms and Adsorbed Mechanism

The first step in the analysis of adsorption isotherm is the visual inspection of its shape and hence identification of the principal mechanism of adsorption (4). Most adsorption isotherms

are grouped into the six types (3). Fig.2-2 shows the type of gas adsorption isotherms.

The type II adsorption isotherm is the normal shape of adsorption isotherms which are given by the adsorption on non-porous materials or macroporous materials. The existence of well-defined point B in Fig.2-2 indicates completion of monolayer coverage and the onset of multilayer development (4).

The type III adsorption isotherm is generally appeared with weak interaction between adsorbent (solid) and adsorbate (gas) and relatively strong interaction in inter adsorbate (gas) molecules. In this case a cooperative effect leads to the development of multilayers before a uniform monolayer has been forms. The adsorption of water vapor on a non-porous material surface is the best example of this type of adsorption isotherm.

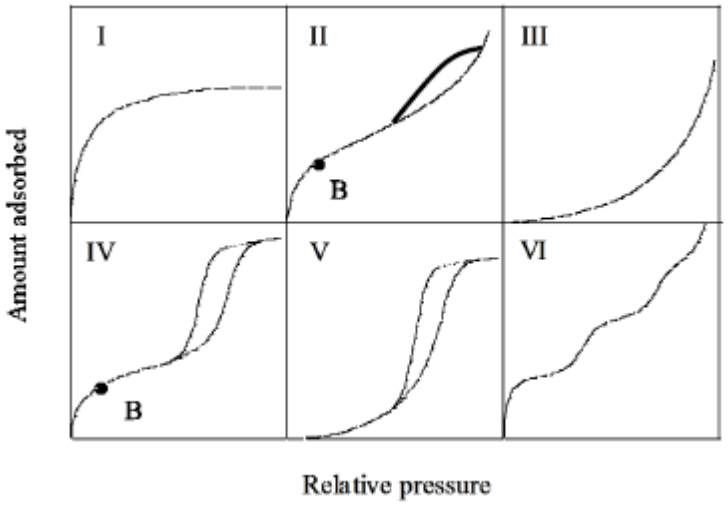

Fig.2-2; Type of gas adsorption isotherms

Type IV adsorption isotherm have unique character; hysteresis loop which is associated with capillary condensation in mesopores (4) and the plateau at high P/P_0 The initial part of the adsorption isotherm is the same shape as the corresponding type II adsorption isotherm and is therefore the result of monolayer, multilayer on the mesopore walls. However after the

appearance uniform mesoporous materials like FSM-16, MCM-41 (5, 6), and the hysteresis loop does not appear on adsorption isotherm even if the adsorbent have mesopores. I would like to refer the mechanism of hysteresis loop at following section; Mesopore Characterization

Type I adsorption isotherm is given by a microporous materials having a small external area. The extreme steep region at low P/P_0 is due to the filling of very narrow pore and the limiting uptake is dependent on the accessible micropore volume (7). Generally Nitrogen has been used as gas (adsorbate) for gas adsorption method. Recently helium gas is also used for characterization of micropore as adsorbate, especially for characterizing ultramicropore (8).

Type VI adsorption isotherm is also uncommon: it represents stepwise multilayer adsorption on a uniform non-porous surface such as graphitized carbon. The stepheight provides a measure of the capacity for each adsorbed layer and in the simplest case it remains nearly constant over two or more adsorbed layers.

Determination of Surface Area

For the determination of specific surface area of porous materials, the Brunauer-Emmett-Teller (BET) method has been widely used (9). This method was constructed based on the Langmuir adsorption mechanism. But the method has some limitations, especially when applied to the materials which has large amount of micropore and ultramicropore like activated carbon (4). The main assumptions by Brunauer-Emmett-Teller in their extension of the Langmuir mechanism to multilayer adsorption are that the localized adsorption happens on an location of surface sites of uniform energy, molecules in the first layer act as sites for molecules in the second and higher layers and the evaporation and condensation properties of all layers are same state of the liquid adsorbate. According to these assumptions, under the steady-state conditions, the rates of condensation (adsorption) and evaporation (desorption) are equal for

each adsorbed layer.

The well-known BET equation is obtained.

$$\frac{P}{n(P_0 - P)} = \frac{1}{n_m C} + \frac{C-1}{n_m C} \cdot \frac{p}{p_0} \qquad (2\text{-}4)$$

where n_m is the monolayer capacity and C is a constant which is related to exponentially to the heat of first layer adsorption.

According to equation (2-4), the plot of $P/n(P_0\text{-}P)$ against P/P_0 should be linear. From the slope and intercept it should be easy to calculate both n_m and C. In fact, the linearity of BET plot is always restricted to certain P/P_0 range of the adsorption isotherm (4). In many cases, the linearity range is about P/P_0= 0.05 - 0.3. But in case of microporous materials like activated carbon, the linear BET plot are just given only below P/P_0=0.1.

The main target of BET method is to calculate the surface area, A_{BET}, from n_m. This step obviously requires prior knowledge of average area a_m occupied by the adsorbate molecule in the completed monolayer. So A_{BET} is expressed as follows.

$$A_{BET} = n_m L a_m \qquad (2\text{-}5)$$

where L is the Avogadro number.

Nitrogen adsorption at 77 K is generally considered to be a suitable adsorbate for surface area determination and it is usually assumed that the nitrogen monolayer is closed packing state, so that a_m (N_2) = 0.162 nm^2 (10).

These BET analysis is commonly available for non-porous materials, mesoporous materials, macroporous materials. In case of microporous materials, BET analysis is inconsistent with reality.

An alternative analysis method is more empirical and is based on the concept of the standard adsorption isotherms (1, 4, 11). To eradicate the influence of energetic surface heterogeneity, material having similar chemical nature of surface is chosen as reference. Non-porous materials are ordinarily used. It has been found convenient to express the reduced adsorption as n/n_s (= α_s), where n_s is the amount adsorbed at certain pre-fixed P/P_0. These normalized adsorption isotherms have been constructed for a number of different systems including adsorption of nitrogen by non-porous materials (12, 13).

We can determine α_s to any P/P_0. But in practice it is usually convenient to take α_s=1 at P/P_0=0.4 (14). So the value is calculated by the following equation (2-6).

$$\alpha_s = \frac{W_{P/P_0}}{W_{P/P_0=0.4}} \qquad (2\text{-}6)$$

where $W_{P/P0=0.4}$ is the amount adsorbed on the standard adsorption isotherm at P/P_0=0.4. $W_{P/P0}$ is the amount adsorbed of the adsorbent under the investigation.

This α_s method consists of plotting the amount adsorbed by the adsorbent under investigation ($W_{P/P0}$) against α_s. We can obtain the slope of standard material $b_{\alpha r}$, and slope of investigated material $b_{\alpha s}$. These two slops have following relation to surface area of standard (a_r) and investigated materials (a_s).

$$\frac{b_{\alpha s}}{b_{\alpha r}} = \frac{a_s}{a_r} \qquad (2\text{-}7)$$

When we know the standard surface area (a_r), we can calculate the surface area of investigated materials by following equation.

$$a_s = \frac{b_{\alpha s}}{b_{\alpha r}} \times a_r \qquad (2\text{-}8)$$

The typical types of α_s-plot are shown in Fig.2-3 (15). A flat surface has a single line passing through the origin. The deviation of α_s-plot from the linearity indicates the occurrence of additional contribution. In case of microporous materials, the line from origin bends to upward in the region of α_s = 0-0.5; f-swing. We can also obtain the micropore volume by extrapolation of the line at high as region; α_s > 1. The intercept of extrapolation give us micropore volume. In case of mesoporous materials, the α_s bends to upward corresponding to capillary condensation. The slope of the line through the origin and the line at high as region gives the total and mesoporous surface area.

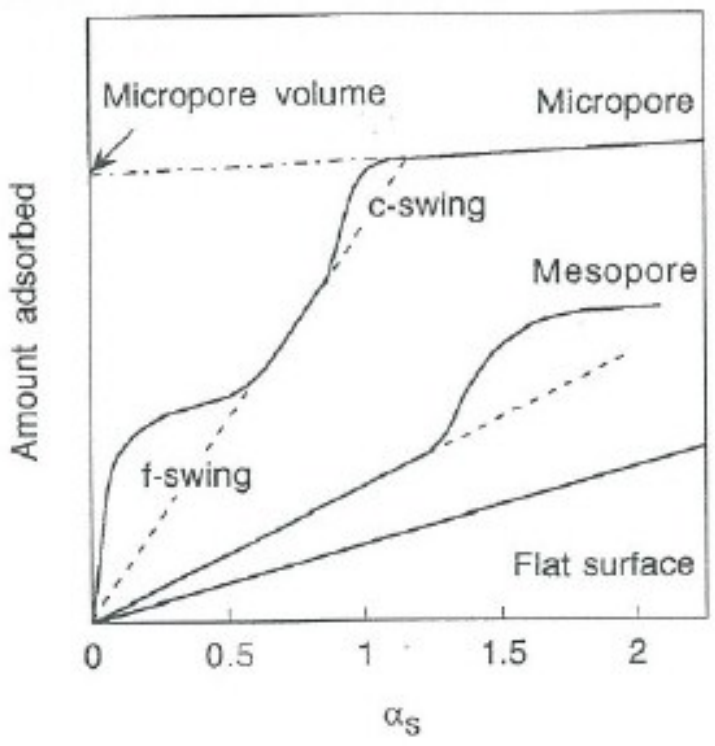

Fig.2-3; Type of α_s-plot

Micropore Characterization

Adsorption mechanism on micropore is pointed out micropore-filling as distinctive mechanism over a lower range of P/P_0 than capillary condensation. But the wider the pore width becomes, the weaker the gas-solid interaction energy is. When the pore width become the two times as large as gas molecule, the gas-solid interaction energy becomes insignificant to occur the micropore filing. In case of small gas molecule like nitrogen, argon, carbon dioxide, it is pointed out that 0.8 nm is upper limit to cause micropore filing. There is an apparent discrepancy of IUPAC classification of micropore.

In order to overcome this discrepancy, alternative approach introduces two kinds of micropore filling mechanisms (16). The first 'primary micropore filling' takes place at very low P/P_0 (e.g. 10^{-5}-10^{-2}) and involves the entry of individual molecules into pores of molecular dimensions. Secondary micropore filling is believed to be a cooperative process, occurring in the wider micropores (which pore width is two-five times of gas molecule) and involving adsorbate-adsorbate interaction or multilayer adsorption. This second pore filling takes place over a much wider range of adsorption isotherm (e.g. $P/P_0 = 10^{-1\text{-}0.3}$), but still before the onset of capillary condensation.

In order to characterize the microporous materials, we have to understand the formulation of the concept of volume-filling as a distinctive mechanism of adsorption. Dubinin and co-workers (17, 18) expressed the functional degree of micropore-filling as in following form which based on the characteristic curve principle of Polanyi (19).

$$\frac{n}{n_P} = \exp[-k(A/\beta)^2] \qquad (2\text{-}9)$$

where A is the affinity or differential free energy of adsorption,

$$A = RT \ln\left(\frac{P}{P_0}\right) \qquad (2\text{-}10)$$

k is a characteristic constant and β is a scaling factor. By combining equation (2-9) and equation (2-10), Dubinin and Radushkevich obtained an equation for micropore filling isotherm, which is usually given in the linear form; DR equation.

$$\log n = \log n_P - B\left(\frac{T}{\beta}\right)^2 \log^2\left(\frac{P_0}{P}\right) \qquad (2\text{-}11)$$

where $B = 2.303R^2/k$

and is considered to be a structural constant, which characterizes the pore structure of the adsorbent.

Equation (2-11) is DR (Dubinin-Radushkevich) equation. The log n against $\log^2 (P_0/P)$ should be linear with the intercept log n_p and slope $-B(T/\beta)^2$. We can determine the only micropore volume from this intercept.

In terms of microporous materials analysis by gas adsorption, Nitrogen molecules are generally used as an adsorbate. As I wrote, the adsorption ability and capacity deeply related with the pore width. The narrower the pore width becomes, the higher the amount adsorbed become. Thus, in order to use porous materials effectively, micropore which pore width is smaller than 0.7 nm; ultramicropore has received much attention.

However the porous materials which have ultramicrepore like low activated carbon have difficulty to characterize its structure by nitrogen adsorption method. This is because nitrogen molecule size is too large to adsorb in the micropore and as a result nitrogen adsorption method can't characterize the pore volume and surface area precisely. The most effective way to characterize these ultramicropore is to use helium atom as an adsorate (20).

The difference between the structures characterized by N_2 and He adsorption by using two

different activated carbon fibers (ACFs) were examined (20).

Fig.2-4 shows the adsorption isotherms of N_2 at 77 K and He at 4.2 K for two different activated ACFs. The W/W_0 means the normalized amount adsorbed which means the amount adsorbed (W) divided by amount adsorbed at P/P_0=1 (20).

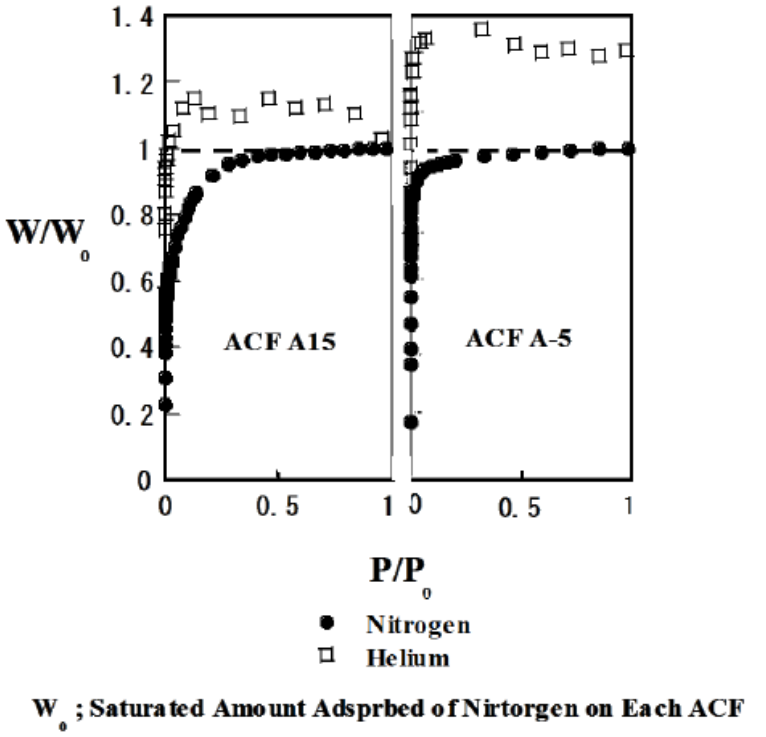

Fig.2-4; Comparison of N_2 and He adsorption isotherms on two different activation ACF

The activation of ACF A-5 is lower than that of ACF A-15. Thus the shape of adsorption isotherm of ACF A-5 is steeper than that of ACF A-15. This adsorption isotherm inspection analysis indicates that ACF A-5 have smaller micropores. The comparison of amount adsorbed of N_2 and He shows that the existence of the pores which He atom can only adsorbed. And the pore volume of ACF A-5 which He atom can only adsorbed reaches 40 % of micropore volume.

The comparison between ACF A-5 and A-15 indicates that the lower activation ACF have the more micropore which N_2 molecules can't adsorbed.

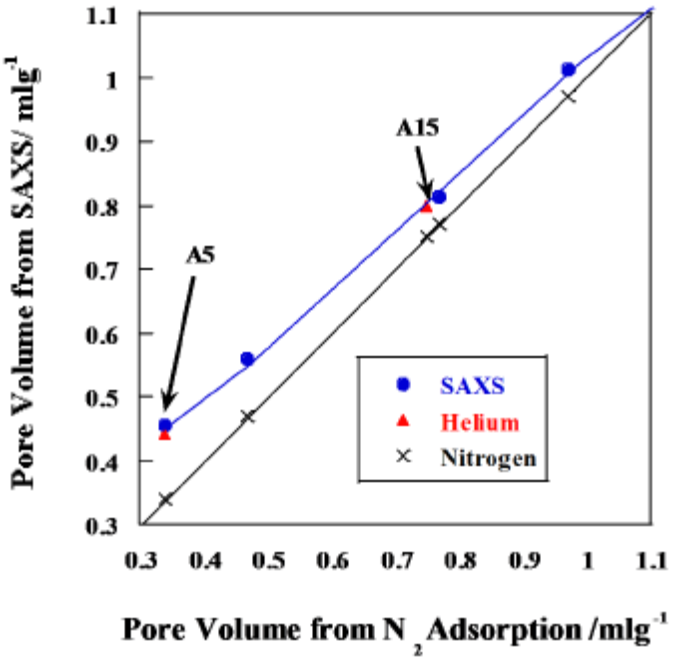

Fig.2-5; The comparison of pore volume characterized by N_2, He adsorption and SAXS

The validity of the pore volume which was calculated by He adsorption was verified. Fig.2-5 shows the pore volume comparison of several different activation ACF between N_2 adsorption, He adsorption and Small angle X-ray Scattering (SAXS). SAXS also used for pore analysis. When there are pore in the materials, the electron density are different between pore region and material regions. By the SAXS measurements, we can get the information of void in porous materials.

Fig.2-5 plots the pore volume calculated by He adsorption on the relation between the pore volume calculated by N_2 adsorption and SAXS (20). The pore volume of ACF A-5 and ACF A-15 calculated by He adsorption accord with the pore volume calculated by SAXS.

Thus, we can say,

- N_2 adsorption is good for characterization of porous materials. But as for ultramicroporous materials like low activated carbon, N_2 adsorption can't characterize these small micropores.
- He adsorption can characterize ultramicropore precisely.
- The validity of pore volume calculated by He adsorption is confirmed by SAXS.

When we characterize the porous materials by gas adsorption, we have to make attention to select the adsorbate properly.

Mesopore Characterization

In the previous section, I wrote the adsorption process in micropore is like volume filling. This process is caused by the strong stable potential in micropore.

In case of mesopores which pore width is 2-50 nm by the classification of IUPAC, there does not have strong stable potential in mesopore and the adsorption process is different from micropore.

The adsorption process of mesopore have been treated as capillary condensation as shown in Fig.2-6-a. The adsorption isotherms of mesoporous materials show type II or type IV adsorption isotherms. From the initial adsorption process, gas molecules adsorb on the mesopore as a shape of condensation. The steep uptake of type II, IV adsorption isotherm at high P/P_0 comes from this condensation in mesopore.

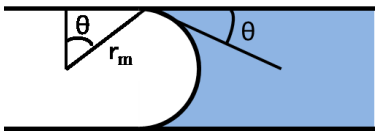

Fig.2-6-a; Adsorption Process in Mesopore

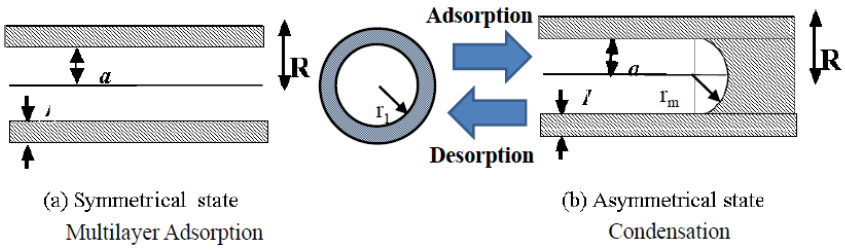

Fig.2-6-b; New Adsorption Process in Mesopore

The evaluation of mesoporosity is based on the following Kelvin equation because the process of adsorption on mesopore has been thought as a shape of condensation.

$$\frac{1}{r_1}+\frac{1}{r_2}=-\frac{RT\cos\theta}{\gamma V_m}\ln\left(\frac{P}{P_0}\right) \qquad (2\text{-}12)$$

where relates the principal radii, r_1 and r_2, of curvature of the liquid meniscus in the pore to the P/P_0 where equilibrium is established with the vapor phase; γ is the surface tension of the liquid condensate and V_m is its molar volume. θ is the contact angle of the meniscus at its line of contact with solid.

The Kelvin equation considered the gas molecule-molecule interaction by surface tension and the molecule-surface interaction by contact angle.

If the pore shape is a cylindrical shape, the pore width d_c is expressed by following equation.

$$d_c = \frac{2\gamma V_m}{RT\cos\theta \ln\left(\frac{P_0}{P}\right)} \qquad (2\text{-}13)$$

The most conspicuous characteristics of type II, IV adsorption isotherms are the existence of hysteresis loop at steep uptake of amount adsorbed at high P/P_0 region. The hysteresis loop means the deviation of adsorption isotherm and desorption isotherm at high P/P_0 steep uptake region.

The existence of adsorption hysteresis have been linked the phenomenon with condensation and evaporation processes in the voids of pores. Kelvin equation (2-12) is expressed by the following way.

$$-\frac{2\gamma V_m \cos\theta}{r_m} = RT\ln\left(\frac{P}{P_0}\right) \qquad (2\text{-}14)$$

where r_m is the mean radius curvature of meniscus, θ is the contact angle of the meniscus at its line of contact with solid.

The hysteresis loop is to be associated with different contact angle of a liquid (condensation phase) in mesopore during condensation (adsorption process) and evaporation process (desorption process) (21). According to this hypothesis, condensation process is essential to make hysteresis loop, but after appearance of uniform mesoporous materials like MCM, FSM, and this hypothesis can't explain all mechanism of hysteresis loop.

In later 1990's, many mesoporous materials which have uniform mesopore were synthesized by molecular template method (5, 6). Some of the N_2 adsorption isotherms of these uniform mesoporous materials don't have hysteresis loop. The N_2 adsorption isotherms have amount adsorbed uptake at certain P/P_0 region. The relationship between hysteresis loop appearance and its pore width was examined and the mechanism of appearance of hysteresis loop was estimated (20).

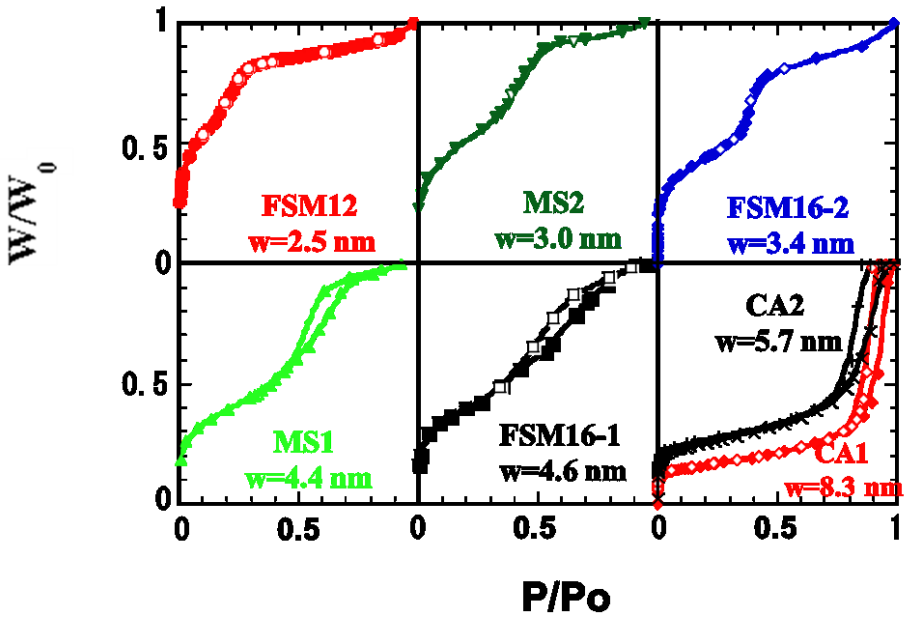

Fig.2-7; Adsorption Isotherms in different pore width mesopore

Fig.2-7 shows the N_2 adsorption isotherms of mesoporous materials which pore widths are 2.5 nm - 8.3 nm. These N_2 adsorption isotherms show that though the porous materials have mesopore, there are the cases that its adsorption isotherms have hysteresis loop. According to these N_2 adsorption isotherms visual inspections, hysteresis loop appear over 3.4 nm pore width range.

In order to understand the hysteresis loop appearance, new adsorption process on mesopore was introduced. The new adsorption process is shown in Fig.2-6-b. According to new process of adsorption, from the initial adsorption process, gas molecules adsorb on the wall of mesopore as a shape of multilayer (symmetrical state). This multilayer adsorption shows the steep increase of adsorbed amount at low P/P_0. After multilayer adsorption, the adsorbed mechanism changes to condensation (Asymmetrical state). The steep uptake of type IV adsorption isotherm at high

P/P_0 comes from this condensation in mesopore.

In addition to introduce this new adsorption process, I applied the Saam-Cole analysis (22) and evaluated the stability of adsorbed phase by potentials (23).

Saam-Cole analysis replaced more microscopic description of molecule-solid interaction and developed the thermodynamic theory with the average molecular potential for liquid phase of adsorbed.

The necessary outline of the Saam-Cole theory and the modified analytical method are described as follows.

The chemical potential change of a multi-layer adsorbed film thickness (l) on a flat surface is given by the Hill's approximation (24).

$$\Delta\mu = U(l) = -\frac{\alpha}{l^3} \qquad (2\text{-}15)$$

where $U(l)$ is the net attractive interaction energy between the adsorbed molecule and surface; α which can be determined by Frankel-Halsey-Hill (FHH) analysis of the adsorption isotherm, is an interaction parameter depending on the molecule and solid. Fig.2-6-b shows the model state of adsorption and desorption in a mesopore whose pore radius is R. The chemical potential change Δμ of the adsorbed molecules in the pore is generally described by the summation of the gas/solid surface ($\Delta\mu_{gas}$) and the interfacial ($\Delta\mu_l$) chemical potential terms.

$$\Delta\mu = \Delta\mu_{gas} + \Delta\mu_i \qquad (2\text{-}16)$$

Here $\Delta\mu_{gas}$ is expressed by equation (2-15). $\Delta\mu_l$ depends on the shape of the meniscus in

the pore. For the transition of multi-layer adsorption to capillary condensation (symmetry-asymmetry transformation), $\Delta\mu_I$ is given by $-\gamma V_m/a$, where γ and V_m denote the surface tension and molar volume of the condensation; a = R-*l* and $r_m=2a$. Because the curvature radius of symmetrical state (a) are *a* and ∞. Thus, the mean curvature radius (r_m) of symmetrical state is calculated as follows.

$$\frac{2}{r_m}=\frac{1}{a}+\frac{1}{\infty}=\frac{1}{a}$$

$$r_m = 2a$$

Hence the chemical potential change of the symmetrical state, $\Delta\mu_s$, is expressed by following

$$\Delta\mu_s = -\frac{\alpha}{(R-a)^3}-\frac{\gamma V_m}{a} \qquad (2\text{-}17)$$

If

$$\left(\frac{\partial\Delta\mu_s}{\partial l}\right)\geq 0$$

the adsorbed film grows; multilayer adsorption

In the case of

$$\left(\frac{\partial\Delta\mu_s}{\partial l}\right)\leq 0$$

the film growth becomes unfavorable, giving rise to the capillary condensation. Hence,

$$\left(\frac{\partial\Delta\mu_s}{\partial l}\right)= 0$$

determines the critical thickness l_c from the symmetry to asymmetry transformation. On the other hand, the chemical potential change of state ($\Delta\mu_a$) for the desorption (asymmetrical state transformation in Fig.2-6-b) is given by following equation.

$$\Delta\mu_a = -\frac{\alpha}{(R-a)^3} - \frac{2\gamma V_m}{a} \quad (2\text{-}18)$$

This is because $r_m = a$ for the symmetry-to-asymmetry transformation. Evaporation needs the condition of

$$\left(\frac{\partial\Delta\mu_a}{\partial l}\right) \leq 0$$

The relation of

$$\left(\frac{\partial\Delta\mu_a}{\partial l}\right) = 0$$

leads to the critical thickness l_e for evaporation. The asymmetric state transforms into the symmetric one at $l = l_c$. If $l_e = l_c$, the adsorption isotherm has no adsorption hysteresis. If $l_c > l_e$, an adsorption hysteresis can be observed.

In order to determine the critical thickness difference Δl_c *(=* l_c - l_e*)*, $\Delta\mu_s$ and $\Delta\mu_a$ must be calculated as a function of l using the FHH plot of the adsorption isotherm, the pore width, and the literature values of γ and V_m. Both of l_c and l_e values can be obtains from the top of the $\Delta\mu_s$ vs. l (eq.2-17) and $\Delta\mu_a$ vs. l (eq.2-18) curves.

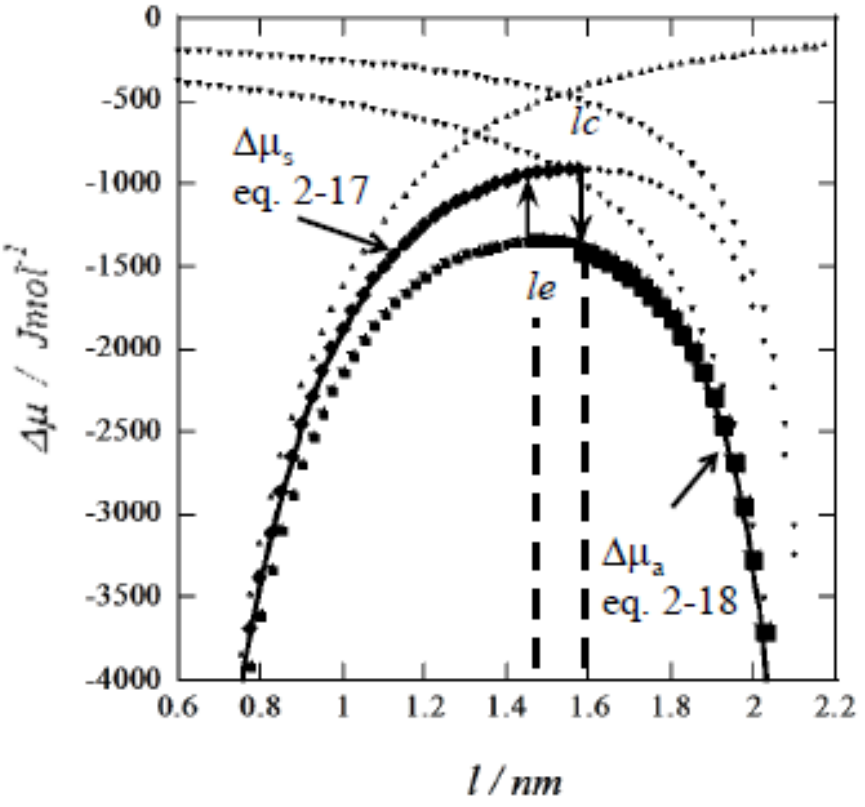

Fig.2-8; Energy Diagram of Adsorbed N_2 in Silicate Pore (MS-1; 4.4 nm)

Fig.2-8 shows $\Delta\mu_s$ vs. l (eq.2-17) and $\Delta\mu_a$ vs. l (eq.2-18) curves of adsorbed N_2 in the silicate porous materials (MS-1; pore width = 4.4 nm). This curve shows the relationship between thickness of adsorbed layer and chemical potential of adsorbed layer in the process of adsorption and desorption. l_c is the adsorbed layer thickness of transforming adsorption form from symmetrical (multi-layer adsorption) to asymmetrical (condensation). l_e is the desorbed thickness of transforming adsorption form from asymmetrical to symmetrical.

Table 2-1 shows the Δl_c of N_2 adsorption on mesoporous materials their pore widths are 2.5 nm-8.3 nm in Fig.2-7. This table indicated that the Δl_c excess 0.1nm, hysteresis loop will appear on adsorption isotherms.

Table2-1; Δl_c and Hysteresis of N_2 Adsorption on Mesopore

Pore width	2.5 nm	3.4 nm	4.4 nm	5.7 nm	8.3 nm
Material		Silicate		Carbon	
Δl_c	0.06 nm	0.09 nm	0.12 nm	0.2 nm	0.22 nm
Hysteresis	×	×	○	○	○

In terms of other gas (adsorbate); He, O_2, Ar, each gas has unique critical thickness difference (Δl_c) and critical pore width for appearance of hysteresis loop.

Fig.2-9 shows the model of Nitrogen molecule adsorption on silicate material surface like FSM, MCM (25, 26). From this model, the thicknesses of N_2 adsorption layer on the surface always have the ambiguity of adsorption layer. The layer thickness ambiguity is about 0.1 nm for N_2 adsorption. In case of N_2 adsorption on mesopore, when Δl_c become less 0.1 nm, adsorption layer thickness would be veiled by the atomic level ambiguity of surface. As a result, N_2 adsorption layer can't recognize the difference of adsorption layer thickness. That means N_2 adsorbed phase recognize $\Delta l = 0$, in case of $\Delta l_c < 0.1$ nm. Thus, adsorption hysteresis would disappear at $\Delta l_c < 0$.

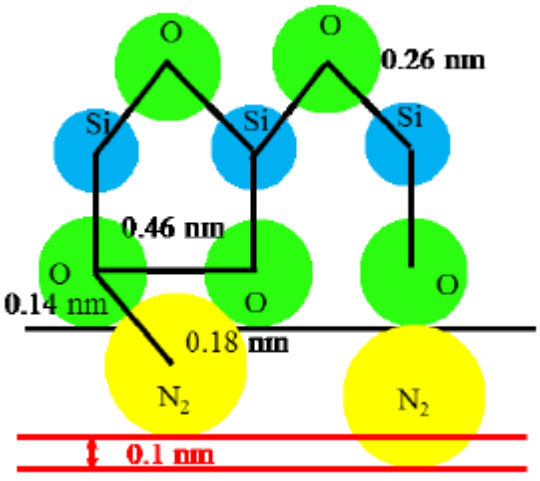

Fig.2-9; Adsorption Model of N_2 on Silicate Adsorbent

Table 2-2 shows the Δl_c and surface ambiguity of N_2, O_2, Ar and He. The boundary Δl_c of hysteresis existence, surface ambiguity and boundary pore width of hysteresis existence shows the good agreement in each adsorbate.

Table2-2; Boundary Δl_c, Pore Width and Surface Ambiguity

	N_2	O_2	Ar	He
Boundary Δl_c (nm)	0.09	0.10	0.10	0.08
Surface Ambiguity (nm)	0.1	0.1	0.09	0.06
Boundary Pore Width (nm)	3.6	2.5	2.5	4.6

2-3.Fundamentals of Liquid Adsorption

Introduction

Adsorption phenomena occur not only at gas-solid but also at liquid-solid interface. As for adsorbate, three states; gas, liquid, solid of materials can be adsorbed (27, 28). These adsorbate adsorption on solid surface have been reported (gas, (4, 29, 30) liquid, (31) dissolved solid). These three adsorption systems explained like as follows (32).

- VPA; vapor or gas phase adsorption on solid surface
- CLA; composite liquid adsorption on solid surface
- SSA; solid solute adsorption on solid surface

Many treatments have been studied and developed to describe these three types of adsorption systems.

As I wrote in a previous section, most of developed treatments of adsorption were about VPA and the applications of gas adsorption have been used in many industrial fields.

In terms of liquid adsorption systems (CLA and SSA), there were not so many studies for treatments though these two adsorption systems are important for application like pollute water purification, poison adsorption and medical use of adsorbents.

CLA adsorption systems usually treat two completely miscible liquid A, B in a series of binary mixtures covering the whole range of possible concentration from pure A to pure B.

In this CLA adsorption systems, it can be expressed the amount adsorbed of A as follows.

$$w_a = \frac{V(x_0 - x)}{M} \qquad (2\text{-}19)$$

where w_a is the amount adsorbed of A, V is the volume of mixture liquid, M is the weight of adsorbent, x_0 is the pre-adsorbed volume rate of A, x is the post-adsorbed volume rate of A.

When the volume rate of A is too small compared with volume B and B does not adsorb on adsorbent, the volume rate A can be displaced by A concentration. Thus we can express the A amount adsorbed in two contents mixture systems as follows.

$$W = \frac{V(C_0 - C)}{M} \qquad (2\text{-}20)$$

where C_0 and C is pre and post adsorption A concentration respectively.

As for SSA, the treatments are different from CLA. Firstly the adsobate is aqueous solutes and is often a micelle. In SSA, adsorbed solutes behave like an adsorbed gas layer, but large difference is a mutual interaction between adsorbed molecules at a high adsorbed amount range.

This solute adsorption is the factor of daily life and the basis of many industries. Its industrial applications include dyeing, detergency, water purification and blood purification.

Thus, this thesis treated this solute adsorption for analyzing the adsorption mechanism of cytokines which are the key protein for controlling inflammatory conditions.

Adsorption Isotherms and its Classification of Solute Adsorption

Possibly the most basic approach to the solute adsorption system is the analysis of adsorption isotherms precisely. In case of solute adsorption, adsorption isotherms is a graph which amount adsorbed is plotted against solute concentration at constant temperature (33).

We can take much information from visual inspection of adsorption isotherms like gas adsorption on adsorbent. Fig.2-9 shows the classification of solute adsorption isotherms (32, 34).

There are 4 classes of adsorption isotherms and each class has several sub groups. The classes were divided by their initial slope and named for convenience the S, L, H and C. S, L class adsorption isotherm have the mechanism like ‘Langmuir’ and H have a high affinity between solute and adsorbent. The C class adsorption isotherm shows the constant adsorbed amount increase with solute concentration.

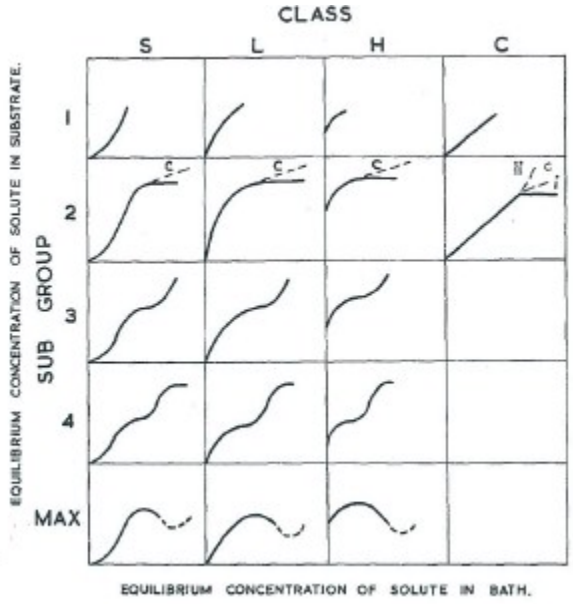

Fig.2-10; Classification of Solute Adsorption Isotherms
C.H. Giles and D. Smith, J. Colloid and Interface Sci., 47, 1974, 755

The major character of S class adsorption isotherm is a low adsorbed amount increase at the low solute concentration. S class adsorption isotherm indicates that there is weak affinity between solute molecules and adsorbent. Thus, the adsorbed amount does not increase at low concentration range. But after some amount of adsorption completed, the amount adsorbed increase steeply. This steep amount adsorbed increase cause by interaction between solute molecules.

L class adsorption isotherm is most popular adsorption isotherm. The affinity between

solute molecules and adsorbent is stronger than that of S class adsorption isotherm. Thus, strong affinity make the adsorbed amount increase steep at low concentration but after some adsorption completed, the occupation of adsorption sites by solute molecules make the increase of amount of adsorbed gentle. At last, the adsorption sites are occupied completely; there appear the flat adsorption isotherm.

H class adsorption isotherm is the special case of L class adsorption isotherm. There is strong affinity between solute molecules and adsorbent. Thus, this strong affinity contributes to the steep amount adsorbed increase at low concentration.

C class adsorption isotherm is consistent with conditions where the number of adsorption sites remains constant throughout the whole range of solute concentrations up to saturation of the substrate.

References

Chapter 2

(1) D.M. Young and A.D. Crowell, Physical adsorption of gases, Butter-Worth, London, 1962. , ASINB: 0000CLJL4

(2) A.V. Kiselev, Discuss Faraday Society, 40, 1965, 205, http://dx.doi: 10.1039/gdf9654000205.

(3) K.S.W. Sing, D.H. Everett, R.A.W. Haul, L. Moscov, R.A. Pieroit, J. Rouquerol and T. Siemieniewska, Pure and Applie Chemistry, 57, 1985, 3603, http://dx.doi:10.1351/pqc198557040603.

(4) S.J. Gregg and K.S.W. Sing, Adsorption, surface area and porosity, Academic press, London, 1982, ISBN: 978-0-123-00956-2.

(5) S. Inagaki, Y. Fukushima, K. Kuroda, Synthesis of highly ordered mesoporous materials from layered polysilicate. J Chem Soc Chem commun 8, 1993,680, http://dx.doi:10.1029/c39930000680.

(6) C.T. Kresge, M.E. Leonowicz, W.J. Roth, J.C. Vartuli, J.S. Beck, Ordered mesoporous molecular sieves synthesized by liquid-crystal template mechanism. 359, 1992, 710-712, http://dx.doi: 10.1038/359710a0.

(7) K.S.W. Sing, Colloids and Surfaces, 38, 1989, 113, http://dx.doi: 10.1016/0166-6622(89)80148-9.

(8) N. Setoyama, Master Thesis of Chiba University, 1993.

(9) S. Brunauer, P.H. Emmett, and E. Teller, J. Am. Chem. Soc., 60, 1938, 309, http://dx.doi:10.1021/ja01145a126.

(10) M.M. Dubinin, in D.H. Everett and R.H. Ottewil, Surface Area Determination, London, Butterworths, 1970, ISBN: 978-0-408-70077-1.

(11) A.L. Mcclellan and H.F. Harnsberger, J. Colloid Interface Sci., 23, 1967, 577, http://dx.doi: 10.1016/0021-9797(67)90204-4.

(12) M.R. Bhambhani, D.A. Cutting and K.W.S. Sing, J. Colloid Interface Sci.,38, 1972, 109, http://dx.doi:10.1016/0021-9797(72)90226-3.

(13) P.J.M. Carrott, R.A. Roberts and K.W.S. Sing, Carbon, 25, 1987, 769, http://dx.doi: 10.1016/0008-6223(87)90148-5.

(14) K.S.W. Sing, in D.H. Everett and R.H. Ottewil, Surface Area Determination, London, Butterworths, 1970.

(15) K. Kaneko, J. Membr. Sci., 96, 1994, 59, http://dx.doi: 10.1016/0376-7388(94)00126-x.

(16) M.M. Dubinin, J. Colloid Interface Sci., 23, 1967, 487, http://dx.doi: 10.1016/0021-9797(67)90195-6.

(17) M.M. Dubinin, Chem. Rev., 60, 1960, 235, http://dx.doi: 10.1021/cr6020a006.

(18) B.P. Bering, M.M. Dubinin and V.V. Serpinsky, J. Colloid Interface Sci., 21, 1966, 378, http://dx.doi: 10.1016/0095-8522(66)90004-3.

(19) M. Polanyi, Ver. Deut. Physic. Ges, 18, 1916, 55.

(20) S. Inoue, Master thesis of Chiba University, 1998.

(21) R. Zsigmondy, Z. Anorg, Allegm. Chem, 71, 1911, 356.

(22) M.W. Cole and W.F. Saam, Phys. Rev. Lett, 32, 1974, 985, http://dx.doi: 10.1131/PhysRevLett.32.985.

(23) S. Inoue, Y. Hanzawa and K. Kaneko, Langmuir, 14, 1998, 3079, http://dx.doi: 10.1021/la971256u

(24) T.L. Hill, Adv Catal., 4, 1952, 211.

(25) P.I. Ravikovitch, S.C.O. Domhnaill, A.V. Neimark, F. Schuch and K.K. Unger, Langmuir, 11, 1995, 4765, http://dx.doi: 10.1021/la00012a030

(26) R.K. Iler, The Chemistry of Silica, Chapter 6, Iohn Wiley & Sons Inc., 1979.

(27) C.H. Giles, Soc. Chem. Ind. Monogr, 37, 1970, 14.

(28) S.J. Gregg, The Surface Chemistry of Solids, Chaman and Hall, London, 1961.

(29) S. Brunaouer, Physical Adsorption of Gases and vapours, Oxford Univ. Press, London, 1968.

(30) J.H. De boer, The Dynamical Character of Adsorption, Oxford Univ. Press, London, 1968.

(31) J.J. Kipling, Adsorption from Solutions of Non-electrolytes, Academic Press, London 1965.

(32) C.H. Giles and D. Smith, J. Colloid and Interface Sci., 47, 1974, 755, http://dx.doi: 10.1016/0021-9797(74)90252-5.

(33) S.D. Forrester and C.H. Giles, Chem. Ind. (London), 831, 1971, 1314.

(34) C.H. Giles, T.H. MacEwan, S.N. Nakhwa and D. Smith, J. Chem. Soc., London, 3973, 1960.

3. Porous materials for blood purification

3-1. Cytokine and Alarmin Adsorption by Activated Carbon

3-1-1. Introduction

Sepsis and systemic inflammatory response syndrome (SIRS) are a consequence of systemic inflammatory responses in intensive care settings and cause subsequent multiple organ failure, which can become uncontrollable and lead to death. The overall mortality rate for sepsis is still high (40 %-80 %) (1-3), and every year, sepsis is a major cause of death in many countries.

It is difficult to determine the cause of a complex inflammatory response, even if a patient develops sepsis and SIRS, and thus select appropriate treatment. The infection of gram-negative bacteria is known to be a major cause of sepsis and SIRS. During the progression of sepsis and SIRS, first tumor necrosis factor-α (TNF-α) and interleukin-1β (IL-1β) are released from leukocytes. Then, IL-6 is released, followed by many other cytokines, and a cytokine cascade is induced. This excessive amount of cytokines makes it difficult to control the inflammatory condition and can eventually lead to multiple organ failure (4-6).

In a recent study, high mobility group box-1 (HMGB1), one of the alarmins, was reported to also be an important mediator in the aggravation of sepsis and SIRS (7). One of the challenges in treating sepsis and SIRS is their complexity. Conventional antibody therapies that have specifically targeted particular mediators, such as IL-1β, IL-6, or TNF-α, have been used; however, their effectiveness in clinical settings has not been verified (8).

Furthermore, extracorporeal blood purification therapies have been performed to remove important mediators from the blood of sepsis and SIRS patients. Continuous hemofiltration and hemodiafiltration are the main methods applied for the removal of cytokines, although their

effectiveness is limited in clinical use (9-12). Other important techniques for mediator removal have also been examined. In particular, adsorption has shown potential for the removal of important mediators from blood (13, 14). Activated carbons (ACs) are conventionally employed as powerful adsorbents in many industrial applications. In the medical field, particularly for blood purification, ACs has been employed for the treatment of poisoning (15, 16).

Additionally, ACs has been considered as adsorbents for cytokines, and their adsorption abilities have been investigated. Specifically, the relationship between the porosity of ACs and their ability to adsorb cytokines has been examined (17-21). Malik et al. concluded that the presence of mesopores is an essential requirement for the adsorption of IL-1β (17). Other successful studies indicated that the relationship between the pore size of the AC and the molecular size of the cytokines influences the adsorption process (18, 19, 20). However, most studies on cytokine adsorption by ACs have focused on specific cytokines such as IL-1β, TNF-α, and IL-6, and the adsorption mechanism has not been investigated.

Inflammatory conditions and multiple organ failure due to sepsis and SIRS result from the excessive immune response of many types of cytokines and alarmins. Therefore, the investigation of the ability of ACs to simultaneously adsorb many different cytokines is important to determine whether ACs is effective adsorbents for the suppression of sepsis and SIRS (5, 8, 22, 23).

The aim of this study, therefore, was to evaluate the ability of a nanoporous AC to adsorb 18 different cytokines and HMGB1, and to clarify the adsorption mechanisms. The 18 cytokines included IL-1β, IL-1ra, IL-4, IL-6, IL-8, IL-10, IL-12, granulocyte colony-stimulating factor (G-CSF), interferon-γ (IFN-γ), interferon-inducible protein-10 (IP-10), monocyte chemotactic protein-1 (MCP-1), macrophage inflammatory protein-1α (MIP-1α), macrophage inflammatory protein-1β (MIP-1β), platelet-derived growth factor (PDGF), TNF-α, vascular endothelial cell

growth factor (VEGF), basic fibroblast growth factor (basic FGF), and regulated on activation normal T-cell expressed and secreted (RANTES). The cytokines and HMGB1 were formulated into inflammatory model plasma prepared via lipopolysaccharide (LPS) administration. The pore structure of the nanoporous ACs and the adsorption isotherms of the 18 cytokines and HMGB1 with different molecular weights on the AC were determined. The adsorption mechanisms for the different cytokines and HMGB1 on the nanoporous AC were studied on the basis of these results.

3-1-2. Experimental

Materials

Pitch-based AC, which is employed in the hemoperfusion column Hemosoba-CHS (Asahi Kasei Medical Co., Ltd., Tokyo, Japan) (AC H-CHS) was used in this study.

Characterization of the H-CHS AC

The surface area and pore size distribution of the AC were determined from the N_2 adsorption isotherm at 77 K using a TriStar II 3020 automatic gas adsorption instrument (Micromeritics Instrument Corporation, Norcross, GA, USA). Prior to the analysis, the H-CHS was dried in vacuum at 473 K for 15 h.

The adsorption isotherms for H-CHS were analyzed using the Brunauer-Emmett-Teller (BET) method (24), the Barrett-Joyner-Halenda (BJH) method (25), and the Dubinin-Radushkevich (DR) method (26) to determine the specific surface area, pore size distribution, and micropore volume, respectively.

Cytokine adsorption experiments

Blood Collection and Inflammatory Model Plasma Preparation

After obtaining approval for this study from the ethics committee of Asahi Kasei Medical Co., Ltd., blood samples from five healthy volunteer donors were collected. LPS (O-127, Sigma-Aldrich Corp., St. Louis, MO, USA) was then administered to the heparinized blood samples at a concentration of 1.0×10^{-4} mg/mL.

After LPS administration, the blood was incubated at 303 K with shaking at 52 rpm for 24 h. Following the centrifugation (2300 G, 10 min) of the blood, inflammatory model plasma was prepared and used for the cytokine adsorption experiments.

The cytokines that were released as a result of the LPS administration were determined prior to the adsorption experiments.

Determination of the Plasma/AC Ratio

To determine the plasma/AC ratio, different amounts of AC were weighed and placed in polypropylene tubes (Falcon™, Becton, Dickinson and Company, Franklin Lakes, NJ, USA). AC was equilibrated in 3.0 mL of a phosphate-buffered saline (PBS) solution overnight, and then the PBS solution was removed. Next, the inflammatory model plasma (3.0 g) was added, and adsorption experiments were performed at 310 K with shaking at 52 rpm for 1 h. The inflammatory model plasma was then collected. The cytokine concentration was determined using an immunoassay method and the HMGB1 concentrations were determined using the enzyme-linked immunosorbent assay (ELISA) method.

The adsorbed quantities of the cytokines and HMGB1 were calculated using the following equation:

$$\text{Adsorption rate (\%)} = \frac{C_A - C_B}{C_B} \times 100, \quad (3\text{-}1\text{-}1)$$

where C_B is the cytokine or HMGB1 concentration in the solution prior to adsorption and C_A is the cytokine or HMGB1 concentration in the solution after the adsorption experiment is completed. The results are listed in Table 3-1-1.

Table 3-1-1; Plasma to H-CHS mass ratios for cytokine adsorption

Plasma (g)	3			
Plasma/AC ratio	3	10	30	60

Cytokine and HMGB1 Adsorption Measurements at 310 K

The adsorption isotherms for the cytokines and HMGB1 were obtained at 310 K by performing batch experiments. Different quantities of H-CHS were each mixed with the inflammatory model plasma (3.0 mL) in polypropylene tubes (15 mL) and then incubated at 310 K with shaking at 52 rpm for 1 h. The inflammatory model plasma was then collected, and the cytokine and HMGB1 concentrations were determined.

The quantities of the adsorbed cytokines and HMGB1 were calculated using the following equation:

$$\text{Adsorption amount (ng/g)} = \frac{(C_A - C_B) \times V_p}{M_{AC}}, \quad (3\text{-}1\text{-}2)$$

where Vp is the volume of the inflammatory model plasma and M_{AC} is the weight of the AC adsorbent.

The adsorption isotherms for the cytokines and HMGB1 were obtained by plotting the adsorption quantity as a function of the equilibrium cytokine concentration in the inflammatory model plasma.

Determination of the cytokine and HMGB1 concentrations

Twenty-four cytokines in the plasma samples were analyzed with the Bio-Plex system (Bio-Rad Laboratories, Hercules, CA, USA): IL-1β, IL-1ra, IL-4, IL-5, IL-6, IL-7, IL-8, IL-9, IL-10, IL-12, IL-13, IL-15, IL-17, basic FGF, G-CSF, IFN-γ, IP-10, MCP-1, MIP-1α, PDGF, MIP-1β, RANTES, TNF-α, and VEGF. The HMGB1 concentration was determined using an ELISA kit (Shino-Test Corporation, Kanagawa, Japan).

3-1-3. Results and Discussion

Fig. 3-1-1 shows the N_2 adsorption isotherm for H-CHS at 77 K. The adsorption isotherm was classified as Type I according to the IUPAC classification system (27). The adsorbed amount increased at a very low relative pressure (P/P_0), suggesting that there were a large number of micropores with pore diameters less than 2 nm. At $P/P_0 = 0.4$, a slight increase in the adsorption quantity was observed along with adsorption hysteresis, suggesting the presence of a small number of mesopores.

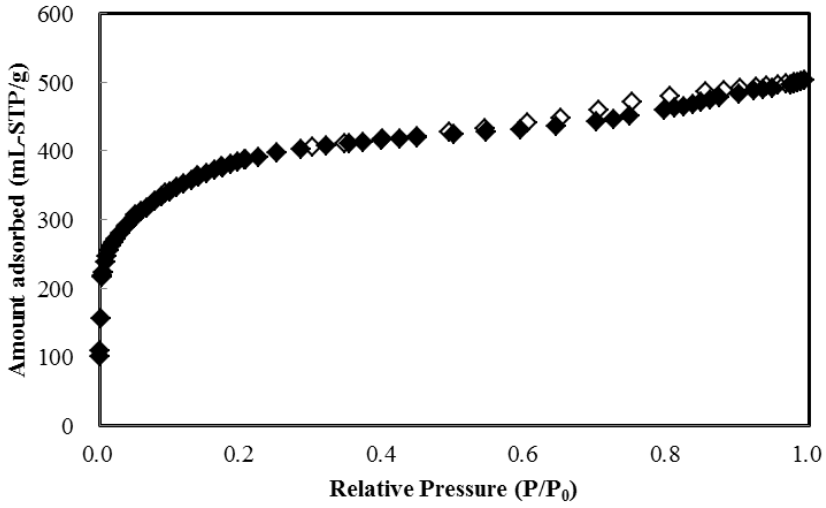

Fig.3-1-1; N_2 adsorption isotherm for H-CHS at 77 K: ◆, adsorption; ◇, desorption.

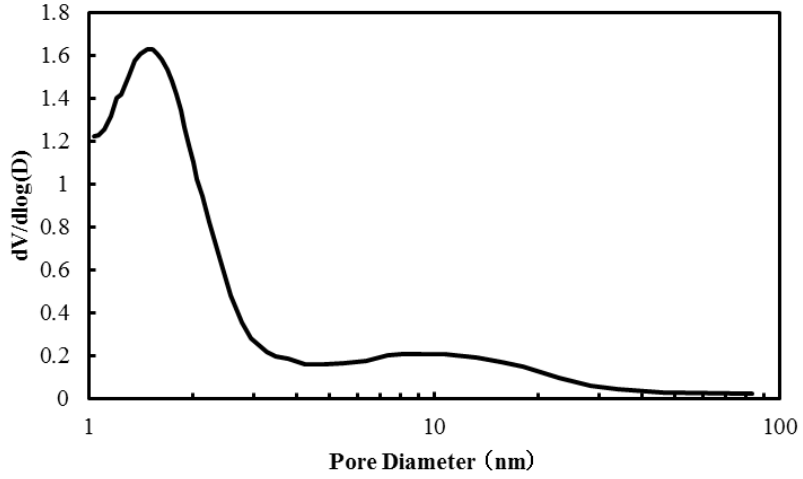

Fig. 3-1-2; Pore size distribution of H-CHS obtained using the BJH method

Fig. 3-1-2 shows the pore size distribution (PSD) curve calculated in the 1-100 nm range using the BJH method. The PSD analysis of H-CHS indicated that its pore structure included micropores and relatively narrow mesopores with diameters of 5–20 nm.

The porosity properties of H-CHS are summarized in Table 3-1-2, including the specific surface area, total pore volume, and micropore volume calculated using the BET equation, the quantity adsorbed at $P/P_0 = 0.99$, and the DR equation, respectively. The specific surface area and pore volumes are typical values for this type of H-CHS. The mean pore diameter, which was calculated using Wick's equation, suggested that the mesopores were not the dominant pore features and was in agreement with the adsorption isotherm data.

Table 3-1-2; H-CHS porosity parameters

BET surface area (m^2/g)	Total pore volume $P/P_0 = 0.99$ (mL/g)	Micropore volume DR analysis (mL/g)	Mean pore width (nm)
1390	0.77	0.53	1.1

The concentrations of 24 cytokines and HMGB1 in the inflammatory model plasma before and after LPS administration are presented in Table 3-1-3. Six of the cytokines (IL-5, IL-7, IL-9, IL-13, IL-15, and IL-17) exhibited slight increase in concentration even after LPS administration. Previously, it was reported that four of these six cytokines were not released even after the administration of gram-negative bacteria (LPS) (28).

Consequently, the adsorption rates of HMGB1 and 18 cytokines were investigated: IL-1β, IL-1ra, IL-4, IL-6, IL-8, IL-10, IL-12, basic FGF, G-CSF, IFN-γ, IP-10, MCP-1, MIP-1α, PDGF, MIP-1β, RANTES, TNF-α, and VEGF. Fig. 3-1-3 shows the relationship between the molecular weight of the cytokines and their adsorption rates for plasma to AC mass ratios (plasma/AC ratios) of 3, 10, 30, and 60. The H-CHS adsorbed all 18 cytokines and HMGB1 from the inflammatory model plasma. However, the adsorption rate depended on the molecular weight at every plasma/AC ratio. Notably, heavier (larger) cytokines exhibited a lower adsorption rate.

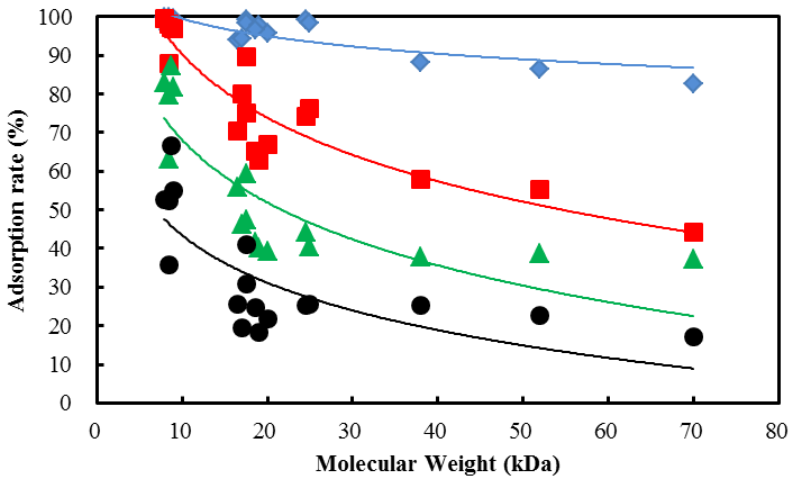

Fig.3-1-3; Molecular weight dependence of the cytokine adsorption rate (5 donor average) on AC. Plasma to H-CHS mass ratio (plasma/AC ratio): ♦, 3; ■, 10; ▲, 30; and ●, 60

Table 3-1-3; Cytokine and HMGB1 concentrations in normal human plasma and inflammatory model plasma

		Plasma mean concentration ±SD(n = 5)	
	Molecular weight (kDa)	Pre-LPS addition (pg/mL)	24 h after LPS addition (pg/mL)
IL-1ß	17.5	5.7 ± 11.4	2930 ± 1620
IL-1ra	17.5	214 ± 179	7810 ± 3120
IL-4	20	1.9 ± 0.6	77.0 ± 8.4
IL-5	50	2.3 ± 2.3	3.8 ± 1.8
IL-6	24.5	83.5 ± 175	58300 ± 16000
IL-7	17.4	26.3 ± 40.2	40.7 ± 42.5
IL-8	8.4	16.7 ± 7.6	21600 ± 16500
IL-9	14	29.8 ± 33.7	151 ± 32.5
IL-10	18.6	24.7 ± 19.0	1440 ± 608
IL-12	70	143 ± 203	322 ± 137
IL-13	12	14.8 ± 17.9	28.3 ± 7.8
IL-15	15	ND[a]	ND[a]
IL-17	25	150 ± 194	682 ± 54.8
Basic FGF	17	85.8 ± 105	196 ± 24.0
G-CSF	17	49.8 ± 43.8	2230 ± 1030
IFN-γ	16.8	8.7 ± 6.6	910 ± 239
IP-10	8.5	1960 ± 1880	120600 ± 41000
MCP-1	11	62.8 ± 41.8	6880 ± 1870
MIP-1α	8	15.5 ± 15.5	18800 ± 8980
PDGF	24	1400 ± 523	30800 ± 9840
MIP-1ß	8	242 ± 385	117000 ± 55600
RANTES	7.8	8280 ± 2530	104000 ± 62600
TNF-α	51[b]	29.0 ± 39.8	4710 ± 3860
VEGF	38.2	81.8 ± 112	1260 ± 582
HMGB1 (ng/mL)	30	6.1 ± 1.5	69.7 ± 18.3

[a]ND: not detected, [b]TNF-α trimer molecular weight

Fig. 3-1-4 shows the relationship between the adsorption rate and the plasma/AC ratio for four of the cytokines (IL-8 (8 kDa), IL-1β (17.5 kDa), IL-6 (24.5 kDa), and TNF-α (51 kDa, typically exists as a trimer)) and HMGB1 (30 kDa). The cytokines with lower molecular weights, IL-8 and IL-1β, were adsorbed on the AC at high adsorption rates even when the plasma/AC ratio was high. For the larger molecular weight cytokines, a high adsorption rate was observed only when the plasma/AC ratio was low. Figs.3-1-3 and 3-1-4, therefore, indicate that the adsorption mechanisms for the cytokines on the AC differed as a function of their molecular weight.

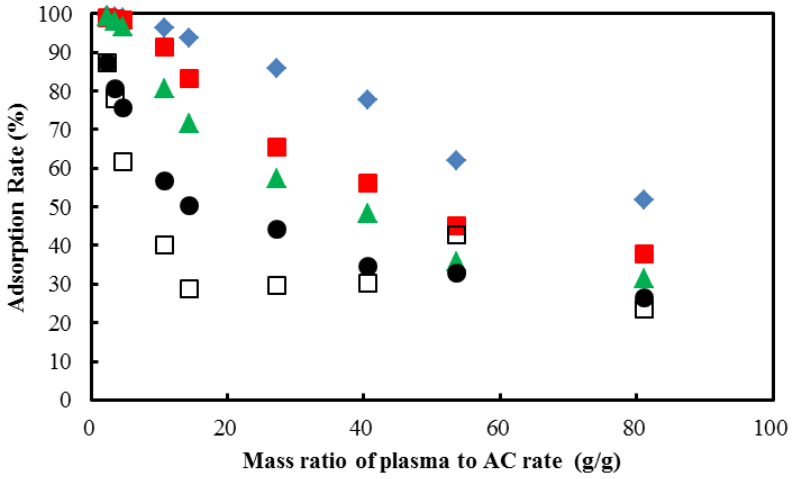

Fig.3-1-4; Dependence of the cytokine adsorption rate (5 donor average) on the plasma to H-CHS mass ratio: ♦, IL-8; ■, IL-1β; ▲, IL-6; □, HMGB1; and ●, TNF-α

Thus, to analyze the adsorption mechanisms of the cytokines and HMGB1, adsorption isotherms for H-CHS were obtained at 310 K. Figs. 5a-e show adsorption isotherms for four cytokines with representative molecular weights and HMGB1 at 310 K.

The shapes of the adsorption isotherms differed with the molecular weight of the adsorbent. According to Giles's classification of liquid adsorption isotherms, IL-8, IL-1β, IL-6, and TNF-α were classified as H-2, L-3, S-3, and S-1 types, respectively (29). The details of the adsorption

mechanisms for the cytokines and HMGB1 were then studied from the shapes of the adsorptions.

Fig.3-1-5a shows the adsorption isotherm for IL-8 and schematic figure of adsorption mechanism. The shape of this adsorption isotherm is classified as H-2 and suggests that the IL-8 molecules strongly interacted with the H-CHS surface. This behavior is due to the relationship between the pore structure and the molecular size of IL-8. H-CHS has mesopores with diameters of 5-20 nm. The volume of the IL-8 (8 kDa) molecule is $4 \times 4 \times 9$ nm^3 (30). The IL-8 molecules can therefore access and be adsorbed in the mesopores of H-CHS, resulting in the acceleration of adsorption due to the adsorption potential field of the mesopores. The other cytokines with a molecular weight of 8-10 kDa (IP-10, MCP-1, MIP-1α, MIP-1β, and RANTES) exhibited similar H-2 type adsorption isotherms, suggesting that the adsorption of these cytokines also occurred via a similar mechanism.

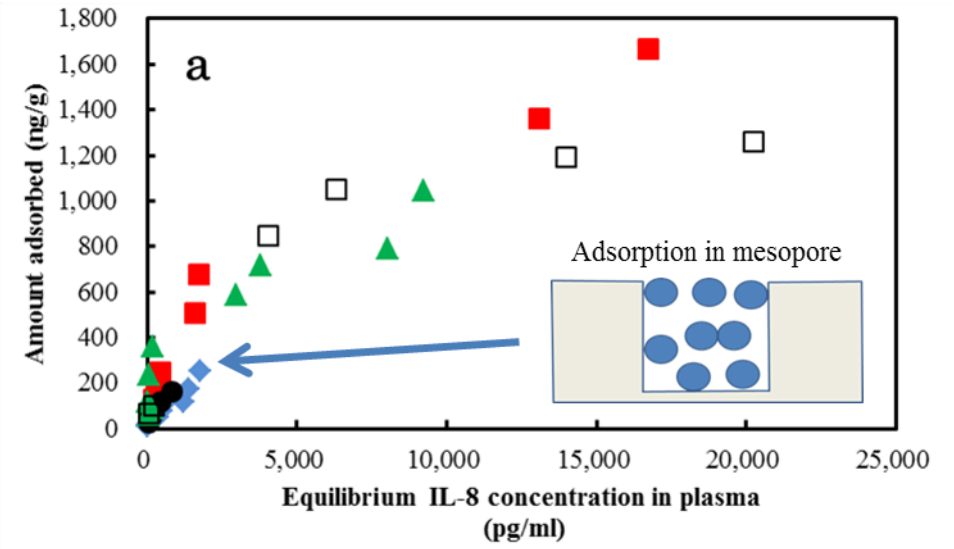

Fig.3-1-5a; Adsorption isotherms for IL-8 in inflammatory model plasma at 310 K: ♦, Donor 1; ■, Donor 2; ▲, Donor 3; ●, Donor 4; and □, Donor 5

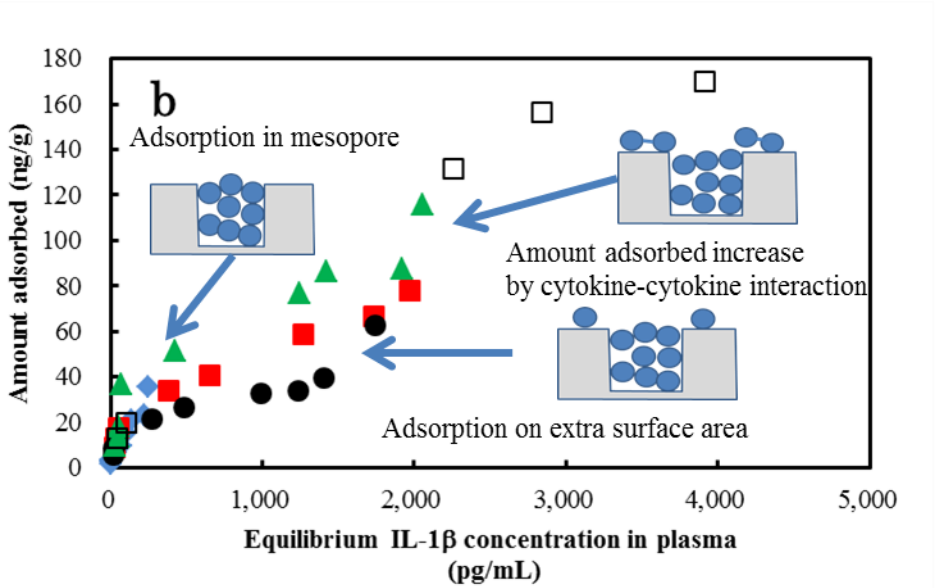

Fig.3-1-5b; Adsorption isotherms for IL-1β in inflammatory model plasma at 310 K: ♦, Donor 1; ■, Donor 2; ▲, Donor 3; ●, Donor 4; and □, Donor 5

Fig. 3-1-5b shows the adsorption isotherm for IL-1β (17.5 kDa), which exhibited an L-3 type isotherm according to Giles's classification and schematic figure of adsorption mechanism. (28). An L-3 type adsorption isotherm suggests that the IL-1β molecules were adsorbed in the mesopores of H-CHS, although the interaction between IL-1β and the surface of H-CHS was weaker than that between IL-8 and the other cytokines with molecular weights of 8–10 kDa because IL-1β is a larger molecule ($5.5 \times 5.5 \times 7.7$ nm^3) (31) and its adsorption in the mesopores of H-CHS was somewhat restricted. As a result, the slope of the adsorption isotherm was gentle at low concentration ranges. Once the mesopores were saturated, IL-1β molecules were able to adsorb on the external surface of H-CHS. However, the slope of the adsorption isotherm was nearly horizontal until a certain concentration was reached because the potential of the external surface was not as strong as that of the mesopores. Notably, at even higher concentrations, the adsorbed quantity increased significantly, suggesting the adsorption of free IL-1β molecules on IL-1β molecules adsorbed on the external surfaces or near the pore

entrances.

The other cytokines with molecular weights of 10-20 kDa (IL-1ra, IL-10, basic FGF, G-CSF, and IFN-γ) also exhibited similar L-3 type adsorption isotherms, indicating that adsorption of these cytokines preceded via the same mechanism as that of IL-1β. It should also be noted that the results of a previous study on the adsorption behavior of IL-1β on a similar mesoporous carbon using a simulated plasma solution containing only the one cytokine agreed well with that obtained for the inflammatory model plasma (17).

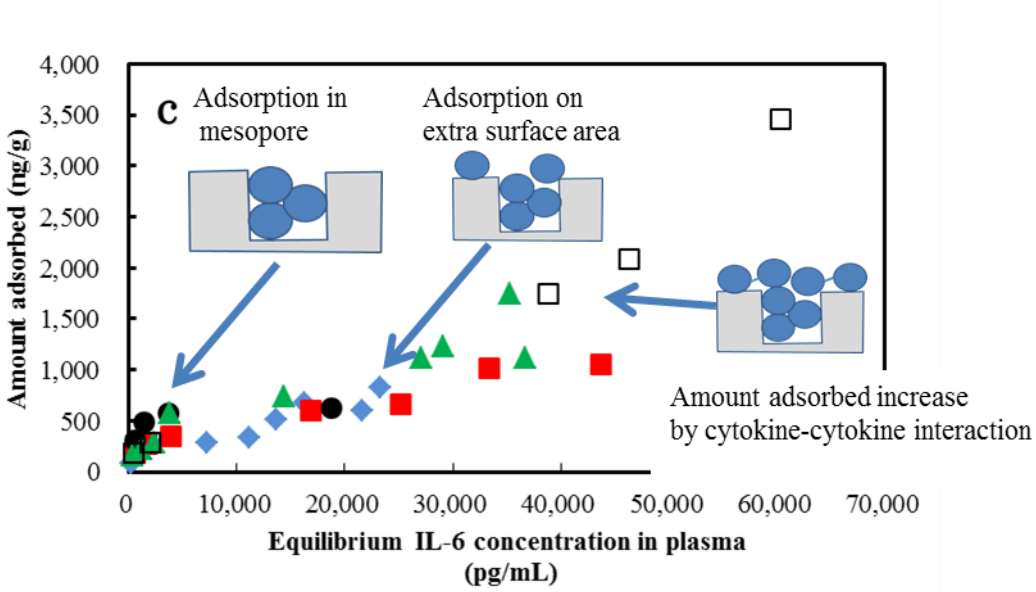

Fig.3-1-5c; Adsorption isotherms for IL-6 in inflammatory model plasma at 310 K: ♦, Donor 1; ■, Donor 2; ▲, Donor 3; ●, Donor 4; and □, Donor 5

As shown in Fig.3-1-5c, the adsorption isotherm for IL-6 (24.5 kDa) was classified as S-3 and schematic figure of adsorption mechanism (29). The adsorption mechanism for S-3 type adsorption isotherms is similar to that for L-3 isotherms, except for the initial slope in the low concentration range. S-3 type adsorption isotherms exhibit a more gradual slope than that of L-3 type adsorption isotherms. Because IL-6 is larger ($5 \times 5 \times 12.2$ nm^3) than IL-1β, it is more difficult for IL-6 to access and be adsorbed in the mesopores of H-CHS (32). However, once

adsorption in the mesopores occurred and they became saturated, the IL-6 molecules were adsorbed on the external surface of H-CHS and ultimately adsorption was accelerated because of the interaction between free molecules and adsorbed IL-6 molecules, as was observed for IL-1β. Once again, the other cytokines with similar molecular weights (20-30 kDa; IL-4 and PDGF) also exhibited similar S-3 type adsorption isotherms, suggesting that the same adsorption mechanism as that for IL-6 was involved.

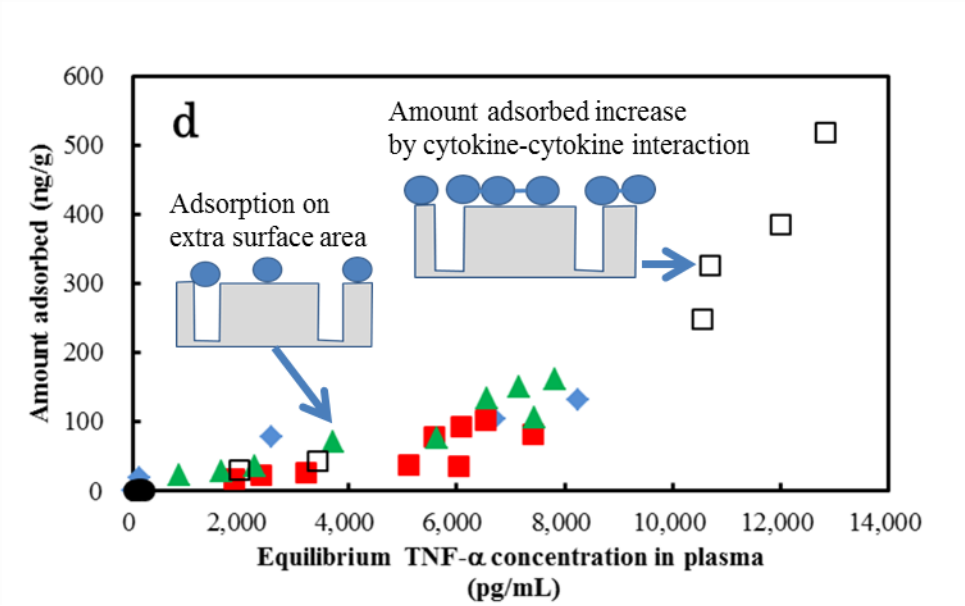

Fig.3-1-5d; Adsorption isotherms for TNF-α in inflammatory model plasma at 310 K: ♦, Donor 1; ■, Donor 2; ▲, Donor 3; ●, Donor 4; and □, Donor 5

Fig.3-1-5d presents the S-1 type adsorption isotherm (29) for TNF-α (51 kDa) and schematic figure of adsorption mechanism, which indicates that the TNF-α molecules were not adsorbed in the mesopores of H-CHS because of the large size of the trimer (9.4 × 9.4 × 11.7 nm^3) (33). The TNF-α trimer was only adsorbed on the external surface of H-CHS. Therefore, the slope of the adsorption isotherm was nearly horizontal over the low concentration range, but then it became steep once a certain concentration was reached, suggesting that interactions between the free and adsorbed TNF-α trimer molecules occurred. Here again, the other

cytokines with molecular weights greater than 30 kDa (IL-12 and VEGF) also exhibited similar S-1 type adsorption isotherms, indicating that the same adsorption mechanism as that for the TNF-α trimer molecules was involved. As expected, the adsorption isotherm for HMGB1 (30 kDa) (Fig.3-1-5e) was also classified as an S-1 type, suggesting that it was adsorbed in the same manner as the TNF-α trimer molecules.

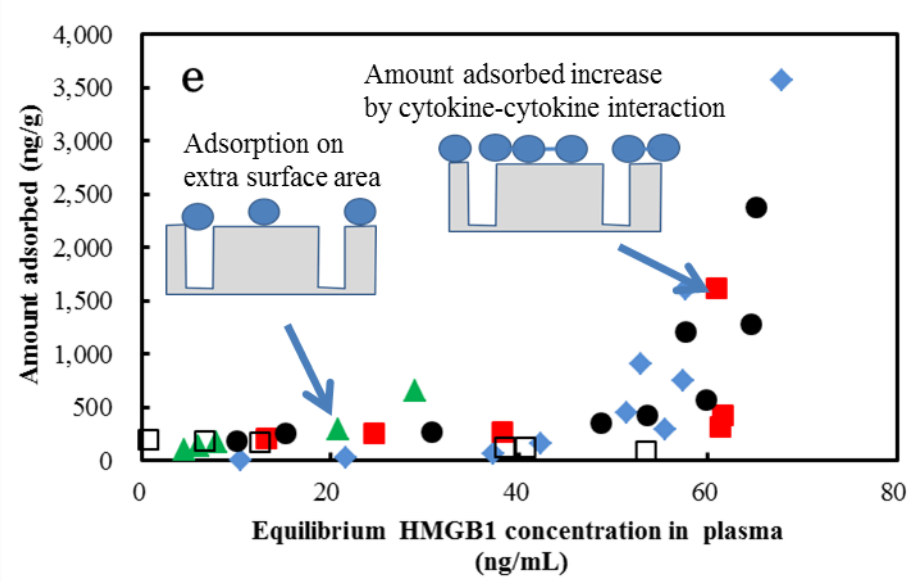

Fig.3-1-5e; Adsorption isotherms for HMGB1 in inflammatory model plasma at 310 K: ♦, Donor 1; ■, Donor 2; ▲, Donor 3; ●, Donor 4; and □, Donor 5

3-1-4. Conclusions

H-CHS, which has micropores and mesopores, was found to adsorb 18 cytokines and HMGB1 from inflammatory model plasma, and the adsorption rates depended on the molecular weights of the adsorbents. An analysis of the adsorption isotherms further suggested that the mechanism of adsorption in the mesopores (diameters ranging from 5 to 20 nm) varied depending on the molecular weights of the cytokines and HMGB1. The cytokines with

molecular weights ranging from 8 to 10 kDa and 10 to 30 kDa were able to access and be adsorbed in the mesopores, although access for the larger cytokines was somewhat restricted. Regardless of the size of the cytokines, once the mesopores were saturated (or if the molecules were too large to be adsorbed in them), the cytokines were adsorbed on the external surface of the AC, and these adsorbed cytokines attracted additional free molecules, leading to an increase in the adsorption rate. Notably, while cytokines (and HMGB1) with molecular weights greater than 30 kDa were only adsorbed on the external surface, they were still adsorbed, but at a slower rate. Thus, on the basis of the results of the adsorption isotherm analysis, it can be concluded that the mechanism of adsorption of the cytokines was dependent on both the molecular weight of the cytokines and the pore structure of the AC.

3-1-5. Appendix

The 18 cytokines and HMGB1 adsorption isotherms on H-CHS s were shown by their molecular weight.

8-10 kDa molecular weight cytokine adsorption isotherms

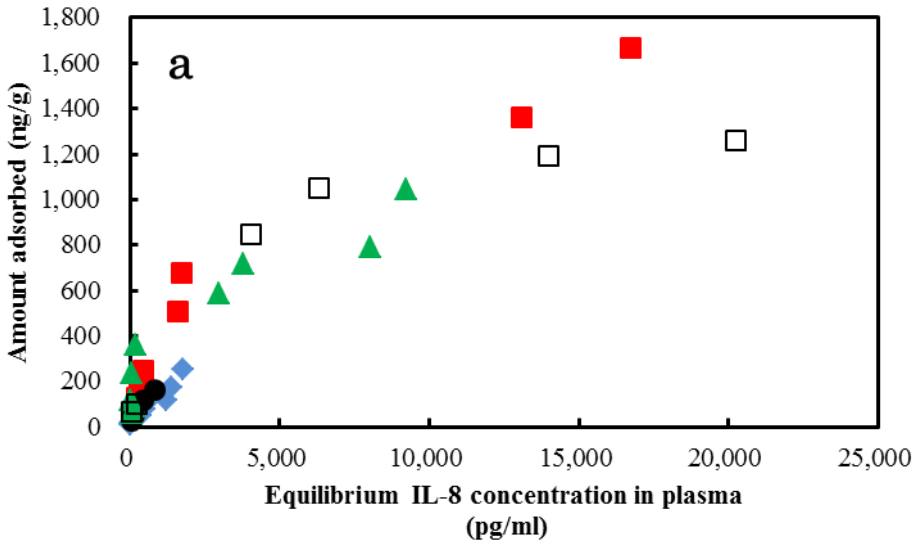

Fig.3-1-5a; Adsorption isotherms for IL-8 (8 kDa) in inflammatory model plasma at 310 K:

♦, Donor 1; ■, Donor 2; ▲, Donor 3; ●, Donor 4; and □, Donor 5

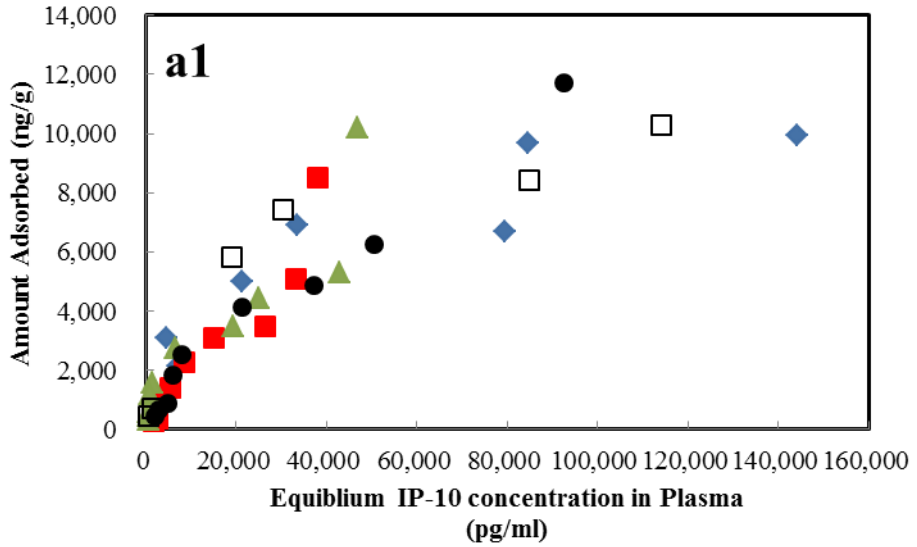

Fig.3-1-5a1; Adsorption isotherms for IP-10 (8.7 kDa)
in inflammatory model plasma at 310 K

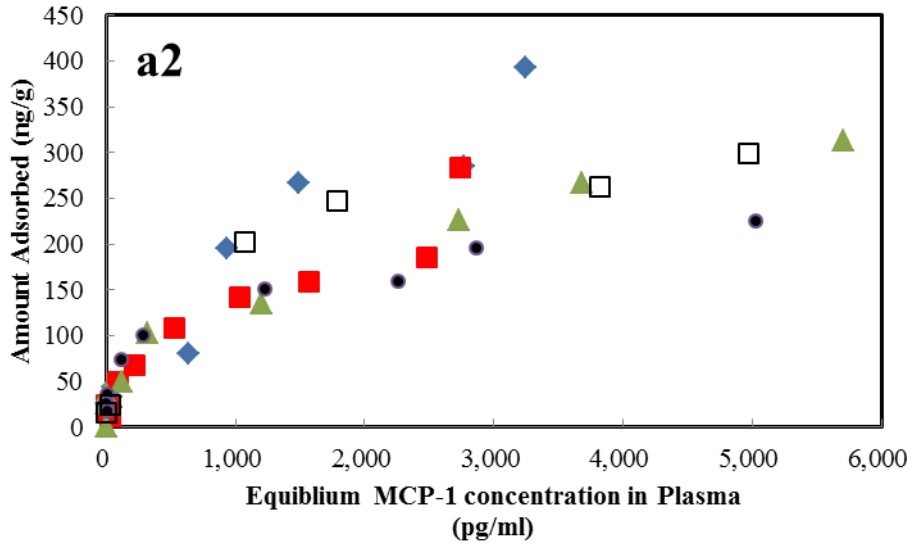

Fig.3-1-5a2; Adsorption isotherms for MCP-1 (8.5 kDa)
in inflammatory model plasma at 310 K

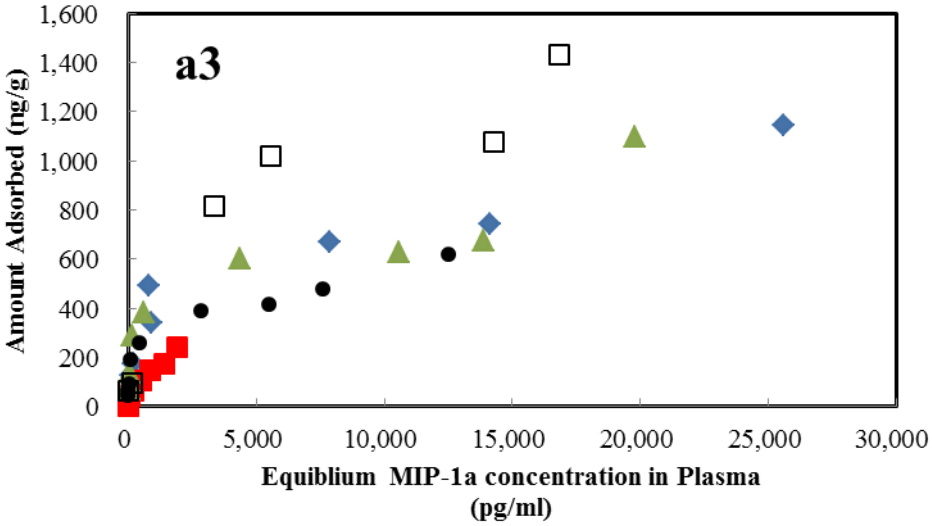

Fig.3-1-5a3; Adsorption isotherms for MIP-1α (8.5 kDa)
in inflammatory model plasma at 310 K

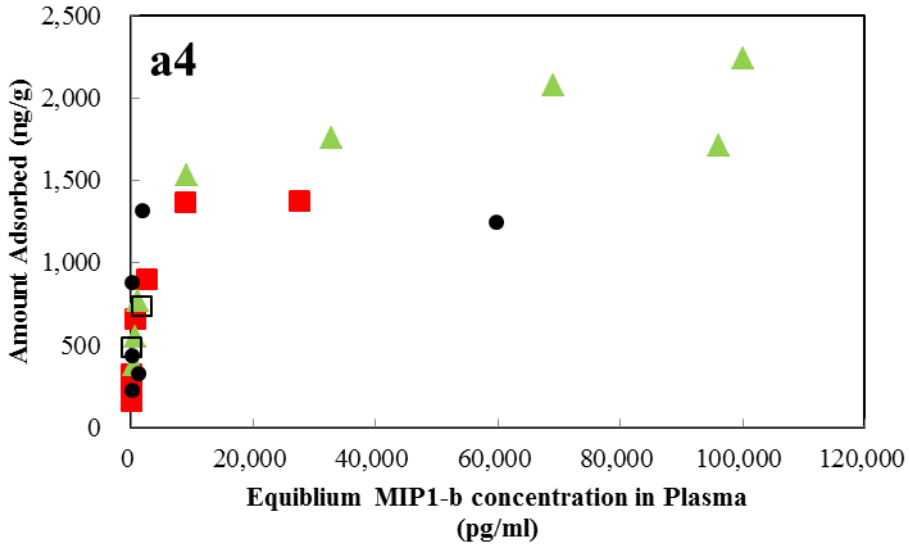

Fig.3-1-5a4; Adsorption isotherms for MIP-1β (8.5 kDa)
in inflammatory model plasma at 310 K

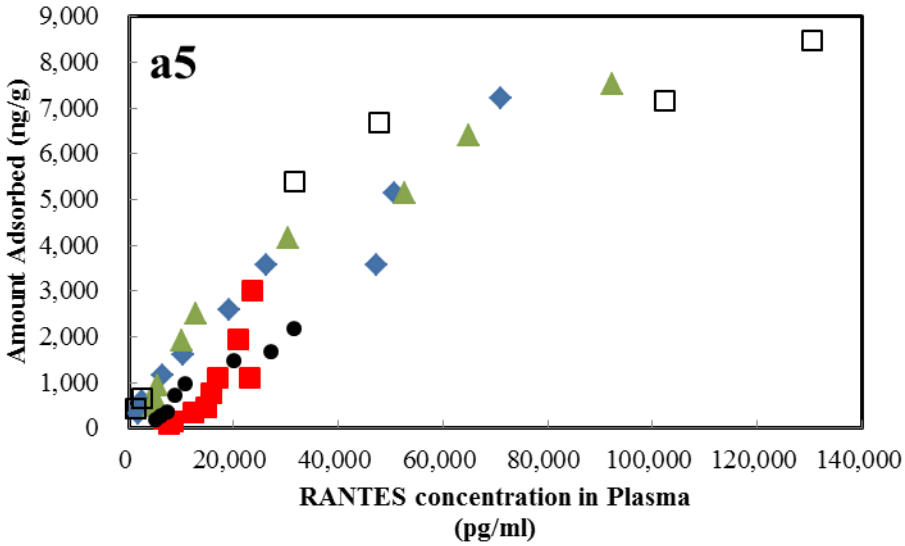

Fig.3-1-5a5; Adsorption isotherms for RANTES (8 kDa)
in inflammatory model plasma at 310 K

10-20 kDa molecular weight cytokine adsorption isotherms

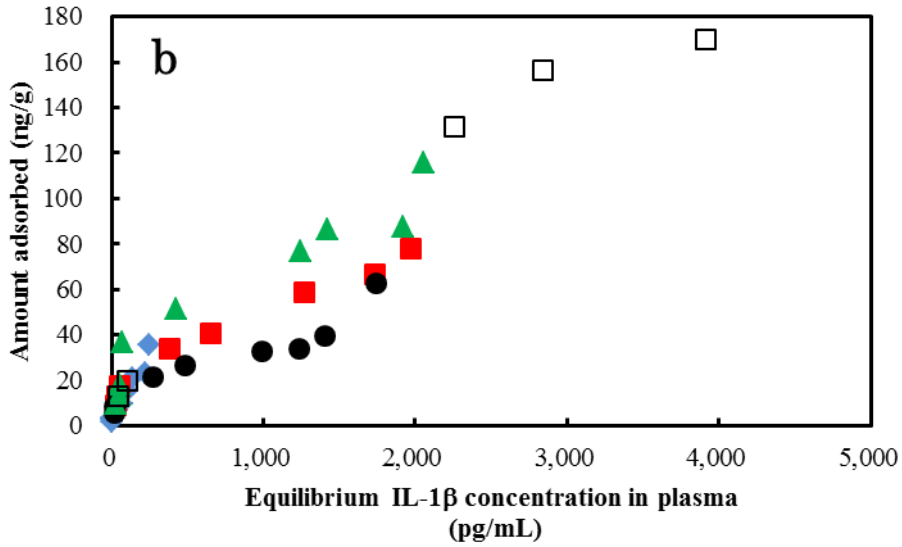

Fig.3-1-5b; Adsorption isotherms for IL-1β (17.5 kDa) in inflammatory model plasma at 310 K:

♦, Donor 1; ■, Donor 2; ▲, Donor 3; ●, Donor 4; and □, Donor 5

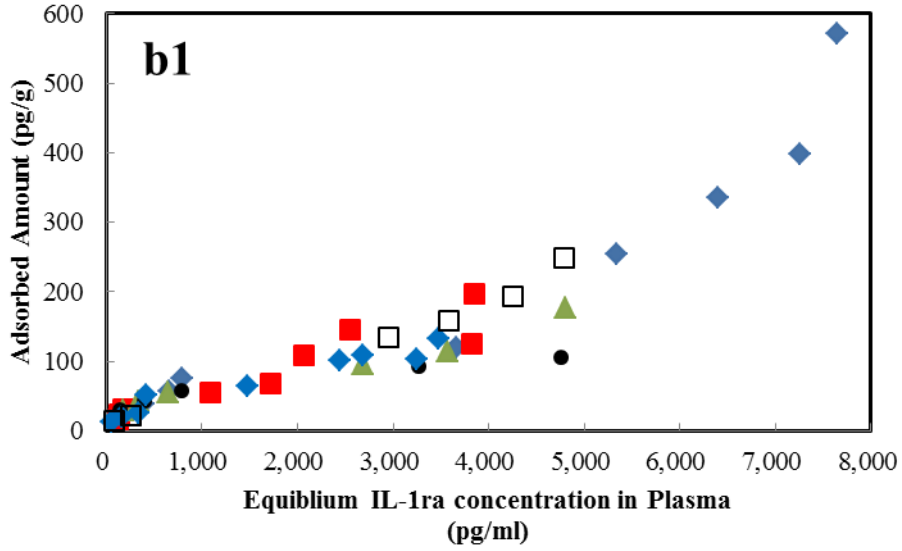

Fig.3-1-5b1; Adsorption isotherms for IL-1ra (17.5 kDa)
in inflammatory model plasma at 310 K

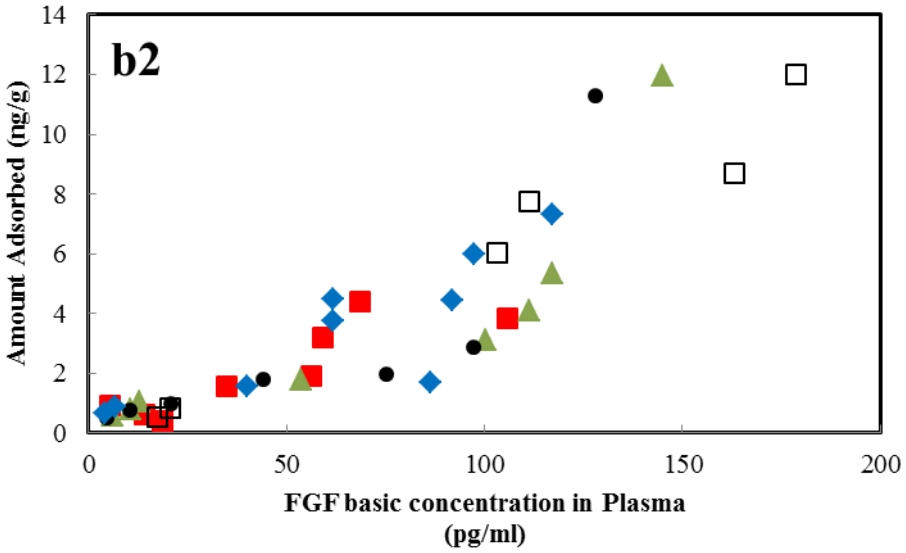

Fig.3-1-5b2; Adsorption isotherms for FGF-basic (16.5 kDa)
in inflammatory model plasma at 310 K

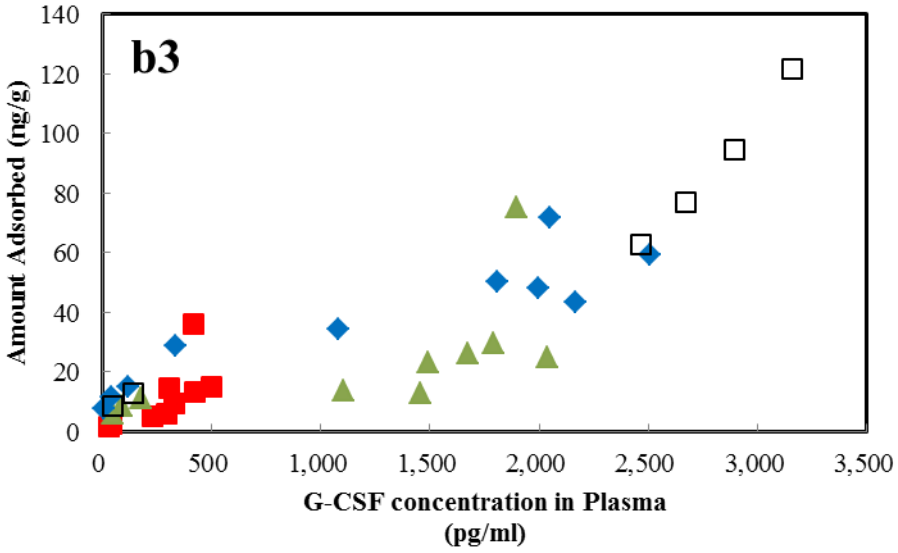

Fig.3-1-5b3; Adsorption isotherms for G-CSF (19 kDa)
in inflammatory model plasma at 310 K

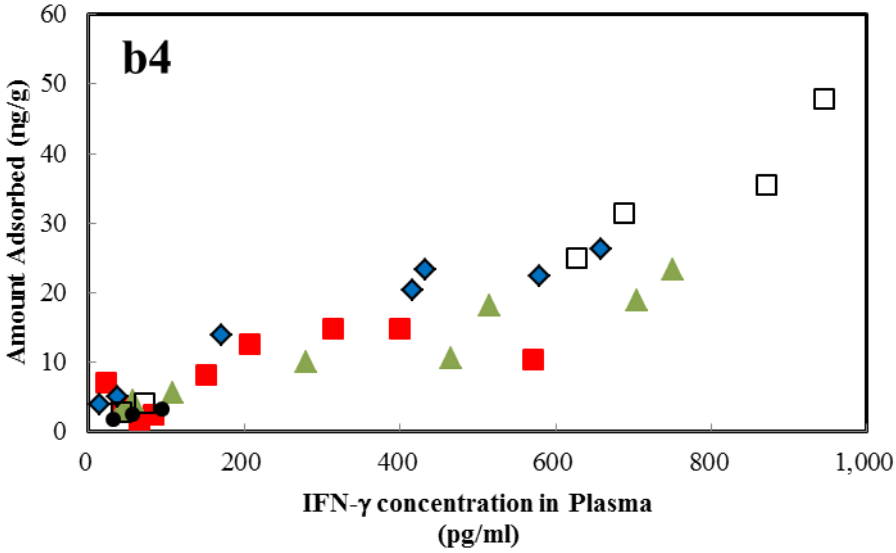

Fig.3-1-5b4; Adsorption isotherms for IFN-γ (17 kDa)
in inflammatory model plasma at 310 K

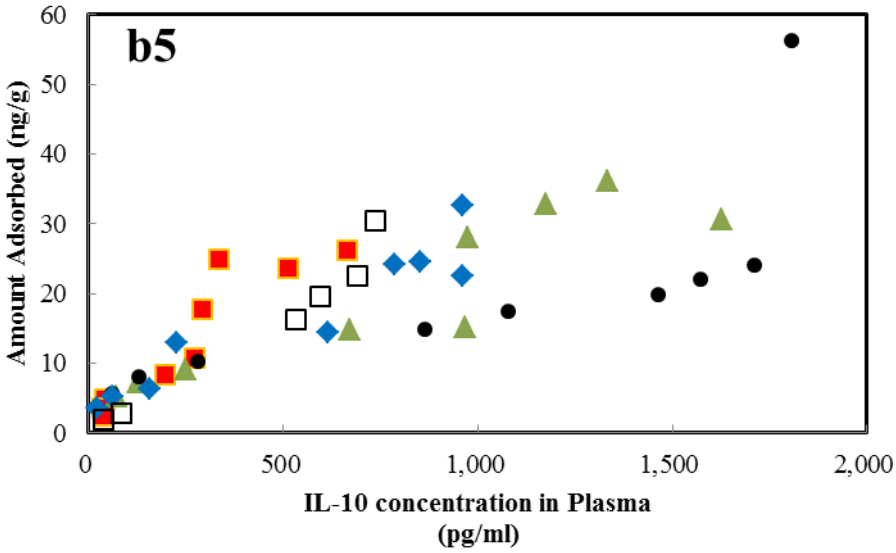

Fig.3-1-5b5; Adsorption isotherms for IL-10 (18.5kDa)
in inflammatory model plasma at 310 K

20-30 kDa molecular weight cytokine adsorption isotherms

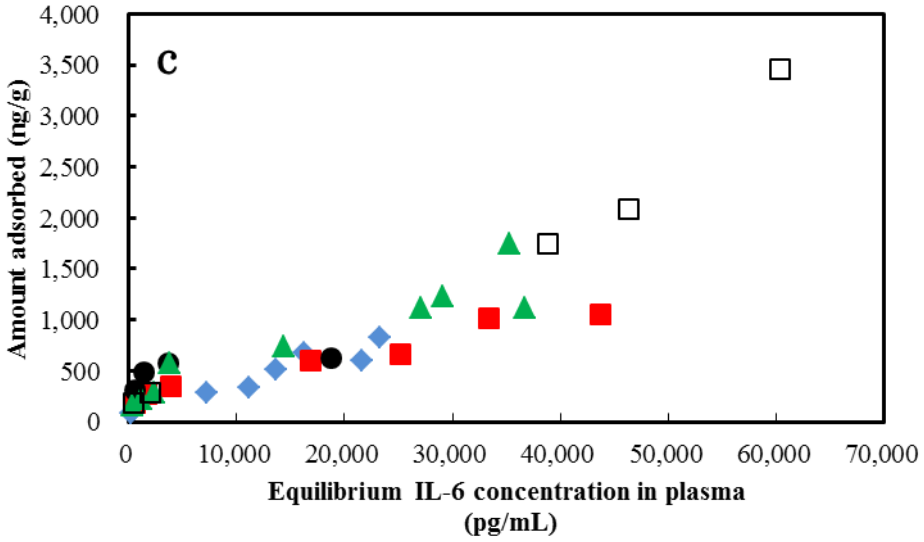

Fig.3-1-5c; Adsorption isotherms for IL-6 (24.5 kDa) in inflammatory model plasma at 310 K:

♦, Donor 1; ■, Donor 2; ▲, Donor 3; ●, Donor 4; and □, Donor 5

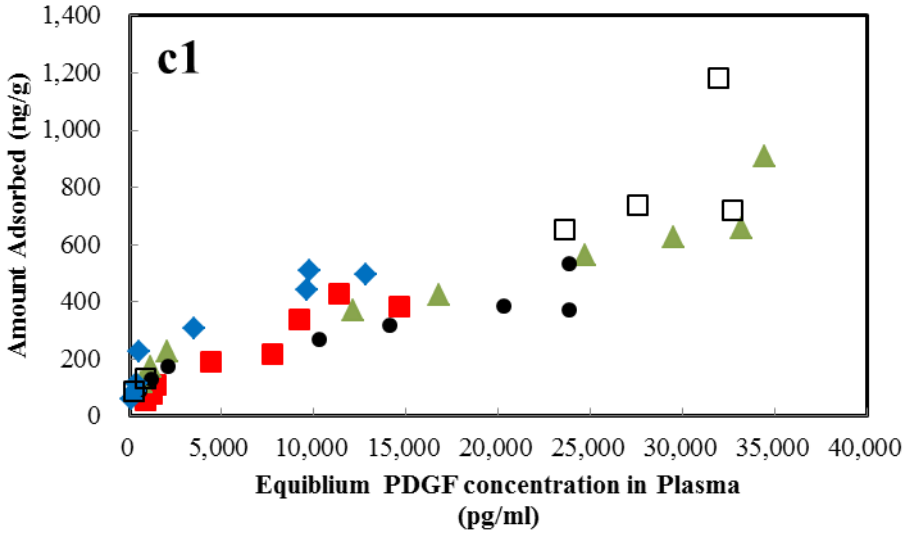

Fig.3-1-5c1; Adsorption isotherms for PDGF (24.9 kDa) in inflammatory model plasma at 310 K

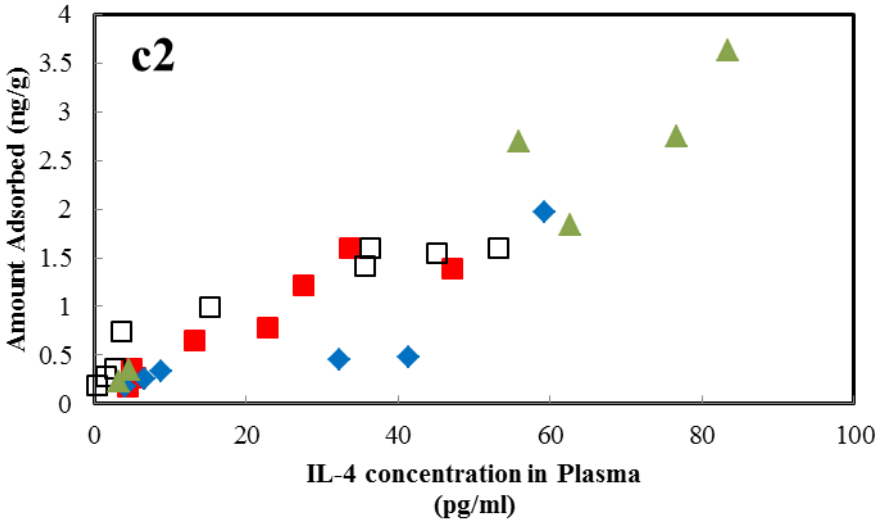

Fig.3-1-5c2; Adsorption isotherms for IL-4 (20 kDa) in inflammatory model plasma at 310 K

Over 30 kDa molecular weight cytokine and HMGB1 adsorption isotherms

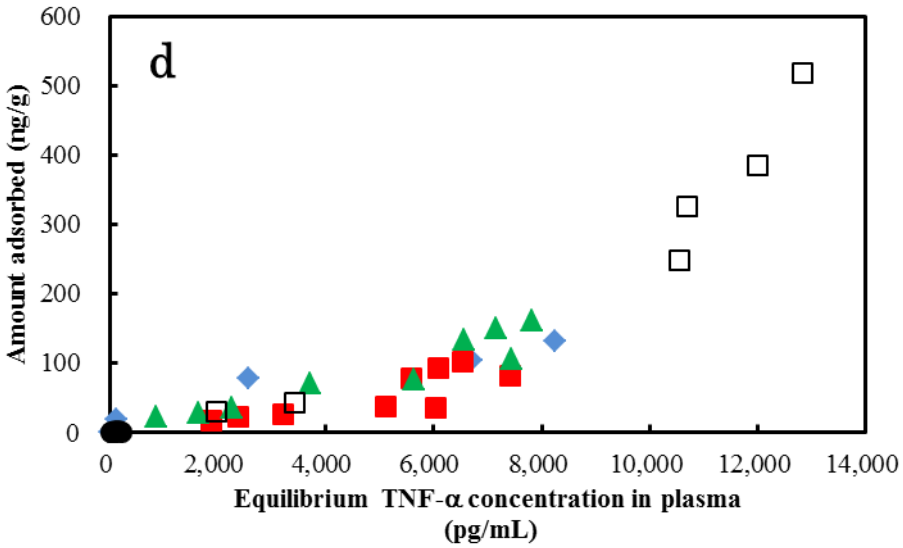

Fig.3-1-5d; Adsorption isotherms for TNF-α (51kDa) in inflammatory model plasma at 310 K:

♦, Donor 1; ■, Donor 2; ▲, Donor 3; ●, Donor 4; and □, Donor 5

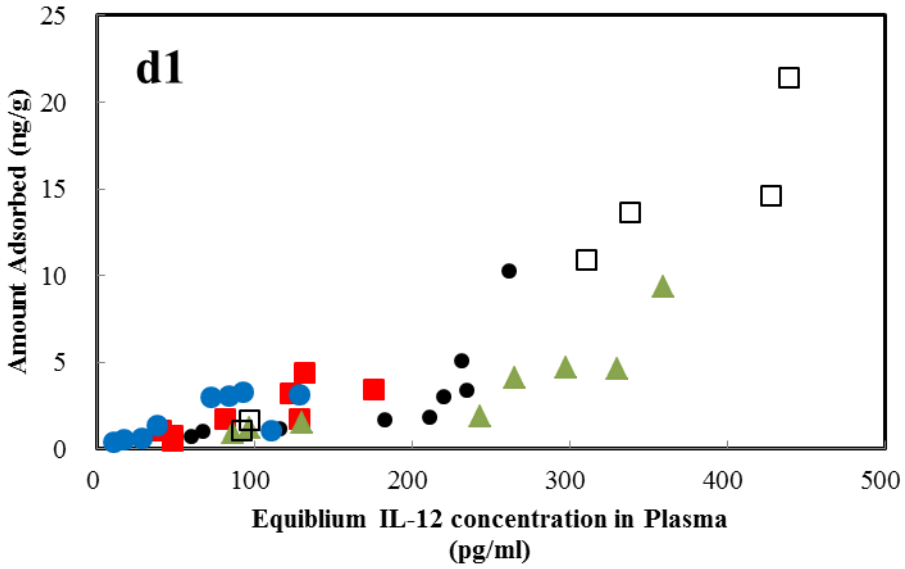

Fig.3-1-5d1; Adsorption isotherms for IL-12 (70 kDa)
in inflammatory model plasma at 310 K

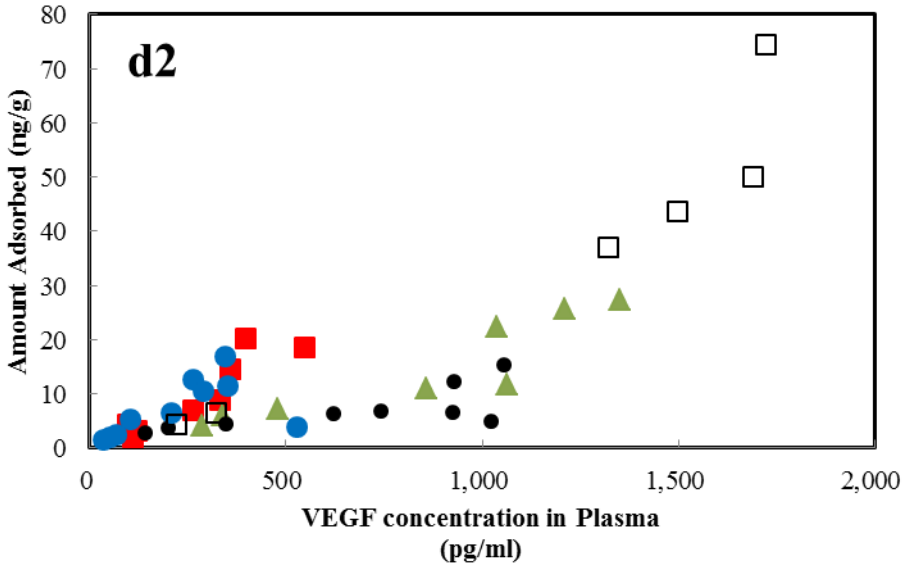

Fig.3-1-5d2; Adsorption isotherms for VEGF (38 kDa) in inflammatory model plasma at 310 K

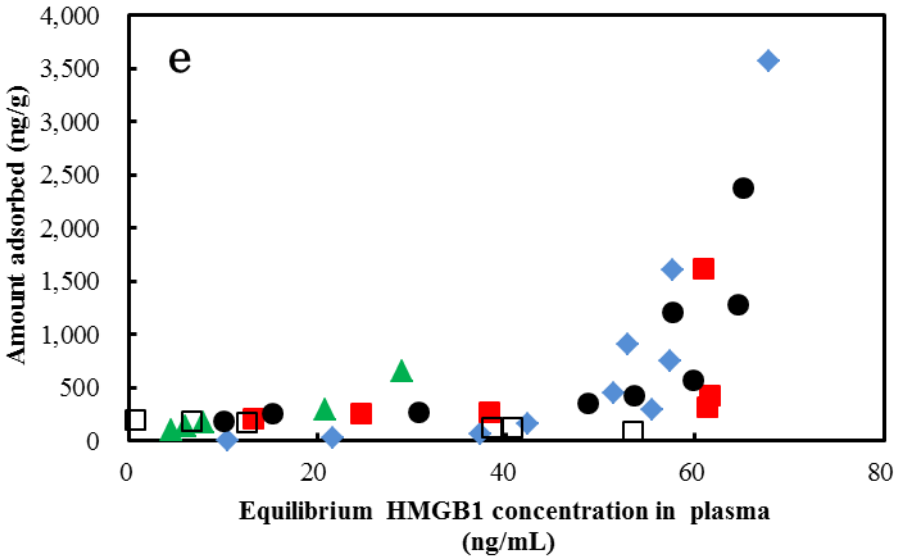

Fig.3-1-5e; Adsorption isotherms for e, HMGB1 (30 kDa) in inflammatory model plasma at 310 K: ♦, Donor 1; ■, Donor 2; ▲, Donor 3; ●, Donor 4; and □, Donor 5

References

Chapter 3-1

(1) E. Slade, P.S. Tamber and J.L. Vincent, Crit. Care, 7, 2003, 1, http://dx.doi: 10.1186/cc1876.

(2) M.D. Williams, L.A. Braum, J. Johnston, R.V. Weiss, R.L. Qualy and W. Linde-Zwirble, Crit. Care, 8 ,2004, R291, http://dx.doi: 10.1186/cc2893.

(3) B.G. Stegmayr, Blood Purificat., 18, 2000, 149, http://dx.doi: 10.1159/000014440.

(4) A. Asachenkov, G. Marchuk, R. Mohler and S. Zuev, IEEE Trans Biomed. Eng., 41, 1994, 943, http://dx.doi: 10.1109/10.324526.

(5) H. Wang and S. Ma, Am. J. Emerg. Med., 26, 2008, 711, http://dx.doi: 10.1016/j.ajem.2007.10.031.

(6) R. Callard, A. Gorge and J. Stark, Immunity, 11, 1999, 507, http://dx.doi: 10.1016/S1074-7613.00. 80125-9.

(7) S. Yamada and I. Maruyama, Clin. Chim. Acta, 375, 2007, 36, http://dx.doi: 10.1016/j.cca.2006.07.019.

(8) D.G. Remick, Curr. Pharm. Design, 9, 2003, 75, http://dx.doi: 10.2174/1381612033392567.

(9) A.S. De Vriese, F.A. Colardyn, J.J. Philippe, R.C. Vanholder, J.H. De Sutter and N.H. Lameire, J. Am. Soc. Nephrol., 10 , 1999, 846.

(10) P. Heering, S. Morgera, F.J. Schmitz, C. Schmitz, R. Willers, H.P. Schultheiss, B.E. Strauer and B. Grabensee, Intensive Care Med., 23 , 1997, 288, http://dx.doi: 10.1007/s001340050330.

(11) A. Sander, W. Armbruster, B. Sander, A.E. Daul, R. Lange and J. Peters, Intensive Care Med., 23 , 1997, 878, http://dx.doi: 10.1007/s001340050425.

(12) E.F.H. van Bommel, C.J. Hesse, N.H.P.M. Jutte, R. Zitse, H.A. Bruining and W. Weimar, Ren. Fail., 19 , 1997, 443, http://dx.doi: 10.3109/08860229709047730.

(13) Y. Kobe, S. Oda, K. Matsuda, M. Nakamura and H. Hirasawa, Blood Purif., 25 , 2007, 446, http://dx.doi: 10.1159/000111568.

(14) S.V. Mikhalovsky, Perfusion-UK 16, 2003, 47, http://dx.doi: 10.1191/0267659103pf627oa.

(15) S.V. Mikhalovsky, S.R. Sandeman, C.A. Howell, G.J Phillips and V.G. Nikolaev, Novel Carbon Adsorbents, Elsevier, 2012 Chapter 21, http://dx.doi: 10.1016/B978-0-08097744-7.00021-1.

(16) S.V. Mikhalovsky and V.G. Nikolaev, Activated Carbon Surface in Environmental Remediation, Elsevier, 2006 Chapter 11 , http://dx.doi: 10.1016/S1573-4285, 06, 80020-7.

(17) D.J. Malik, G.L. Warwick, M. Venturi, M. Streat, K. Hellgardt, N. Hoenich and J.A. Dale, Biomaterials, 25 , 2004, 2933, http://dx.doi: 10.1016/j.biomaterials.2003.09.076.

(18) C.A. Howell, S.R. Sandeman, G.J. Philips, A.W. Lloyd, J.G. Davies, S.V. Mikhalovsky, S.R. Tennison, A.P. Rawlinson, O.P. Kozynchenko, Hannah L.H. Owen, J.D.S. Gaylor, J.J. Rouse and J.M. Courtney, Biomaterials, 27 , 2006, 5286, http://dx.doi: 10.1016/j.biomaterials.2006.05.041.

(19) G. Yushin, E.N. Hoffman, M.W. Barsoum, Y. Gogotisi, C.A. Howell, S.R. Sandman, G.J. Philips, A.W. Lloyd and S.V. Mikhalovsky, Biomaterials, 27 , 2006, 5755, http://dx.doi: 10.1016/j.biomaterials.2006.07.019.

(20) S. Yachamaneni, G. Yushin, S. Yeon, Y. Gogotsi, C. Howell, S. Sandman, G. Philips and S. Mikhalovsky, Biomaterials, 31 , 2010, 4789, http://dx.doi: 10.1016/j.biomaterials.2010.02.054.

(21) C.A. Howell, S.R. Sandman, G.J. Phillips, S.V. Mikhalovsky, S.R. Tennison, A.R. Rawlison and O.P. Kozynchenko, Int. J. Artif. Organs, 36, 2013, 624, http://dx.doi: 10.5301/ijao.5000231.

(22) E. Lin, S.E. Calvano and S.F. Lowry, Surgery, 127, 2000,117, http://dx.doi: 10.1067/msy.2000.101584.

(23) E. Neugebauer, C. Willy and S. Sauerland, Shock, 16, 2001, 252, http://dx.doi: 10.1097/00024382-200116040-00003.

(24) S. Brunauer, P.H. Emmett and E. Teller, J. Am. Chem. Soc., 60 , 1938, 309, http://dx.doi: 10.1021/ja01269a023.

(25) E.P. Barrett, L.S. Joyner and P.P. Halenda, J. Am. Chem. Soc., 73 , 1951, 373, http://dx.doi: 10.1021/ja01145a126.

(26) M.M. Dubinin, Chem. Rev., 60 , 1960, 235, http://dx.doi: 10.1021/cr60204a006

(27) S. Brunauer, L.S. Deming, W.E. Deming and E. Teller, J. Amer. Chem. Soc., 62 , 1940, 1723, http://dx.doi: 10.1021/ja01864a025.

(28) N. Yasuda, K. Goto, S. Yamamoto, S. Hidaka, S. Hagiwara and T. Noguchi, J. Surg. Res., 176 , 2012, 226, http://dx.doi: 10.1016/j.jss.2011.07.047.

(29) C.H. Giles, D. Smith and A. Huitson, J. Colloid Interface Sci., 47 , 1974, 755, http://dx.doi: 10.1016/0021-9797, 74, 90252-5.

(30) K. Rajarathnam, J. Clarklewis and B.D. Sykes, Biochemistry, 34, 1995, 12983, http://dx.doi: 10.1021/bi00040a008.

(31) H. Einspahr, L.L Clancy, S.W. Muchmore, K.D. Watenpaugh, P.K.W. Harris, D.B. Cater, K.A. Curry, C.-S.C. Tomich, A.W. Yem, M.R. DEibel Jr., D.E. Tracey, J.W. Paslay, N.D. Staite, J.B. Cater, N.Y. Theriault, I.M. Reardon, H.A. Zurcher-Neely and R.L.Heinrikson, J. Cryst. Growth, 90, 1988, 180, http://dx.doi: 10.1016/0022-0248, 88, 90313-2.

(32) W. Somers, M. Stahl and J.S. Seehra, Embo. J., 16, 1997, 989 , http://dx.doi: 10.1093/emboj/16.5.989.

(33) C. Reed, Z.Q. Fu, J. Wu, Y.N. Xue, R.W. Harrison, M.J. Chen and I.T.Weber, Protein Eng.,

10 , 1992, 1101, http://dx.doi: 10.1093/protein/10.10.1101.

3-2. Parasite removal by cellulose porous beads

3-2-1. Introduction

Infectious disease is extended by pathogens like viruses, bacteria, proteins, prokaryotes and eukaryotes. There are a lot of infectious disease in the world; Dengue, Chikungunya, HBV (Hepatitis B virus), HCV (Hepatitis C virus), HIV (Human Immunodeficiency virus), Syphilis which are transmitted by virus (1, 2, 3, 4), Babesia, Malaria, Chagas which are transmitted by bacteria or prokaryotes, CJD (Creutzfeldt-Jakob disease) which is transmitted by protein. These infectious diseases have their unique route of infection and expanded in their unique area.

However the development of surgery operation stated to demand blood and blood component drastically. From 1990's there were several suspected cases that transfusion blood and blood components were the cause of transmission of infectious disease. Thus from 1990's, most of European countries, US and Japan started to check the risk of popular infectious disease (HIV, HBV, HCV). But miner infectious disease pathogens are not still checked (5).

In this decade, the number of immigrants from South America and Africa; developing countries, have been increasing. With immigrants' number increase, the risk of local infectious disease like Malaria and Chagas disease by blood transfusion increase.

Chagas disease is one of the most serious diseases to prevent expansion because of the difficulty of detecting technique.

What is Chagas disease?

Chagas disease is one of the local diseases in South America. T*rypanosoma cruzi (T. cruzi)* is the causative agent. A chronic and debilitating systemic disorder affects about 25 million people in Latin America. Chagas disease expands from human to human though vampire insects.

Human immune systems and leukocyte cannot eradicate *T. cruzi* unless we eradicate by medicine or remove *T. cruzi* from blood.

From a clinical point of view, the disease is characterized by an acute phase with high parasite and strong immunosuppression (6, 7) followed by a chronic phase with autoimmune pathology (8, 9). In this chronic phase, people can't realize that they were infected because of non-symptoms. Thus they contribute their blood for blood donation. After this chronic period which is 5~10 years, the strong symptoms like organ hypertrophy and explosion occur suddenly and introduce to death.

Though Chagas disease is serious, there is not effective medicine, treatment and preventive method for transmission by blood transfusion.

Therefore, the materials which can adsorb, remove *T. cruzi* from blood by extracorporeal treatment have been demanded for a long term.

This thesis examined the *T. cruzi* remove method by porous materials which pore size is same as size of *T. cruzi*.

3-2-2. Experimental

Preparation and Characterization of Cellulose Porous Beads (CPB)

T. cruzi can't be removed from blood by filtration without removing red blood cells because size of T. cruzi is smaller than red blood cell and leukocyte. Thus the macroporous materials which have 1-5 μm width pore were needed to prepare. Though there are many kinds of porous materials which have micropore or mesopore, there are few macroporous materials. Fig.3-2-1 shows the relationship among *T. cruzi*, other blood components and pore size of CPB.

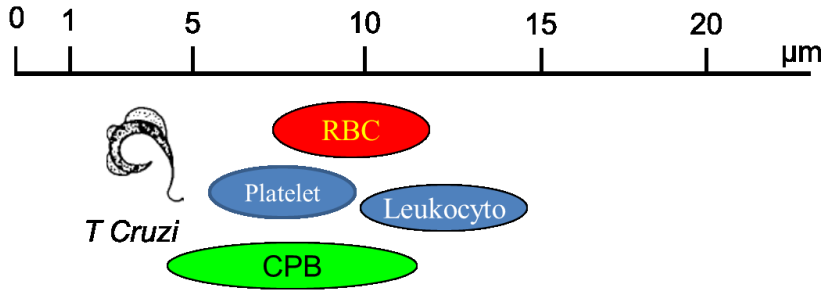

Fig.3-2-1; Size Comparison among *T.cruzi* and Blood Cells

Cellulose porous beads (CPB) (Asahi Kasei medical Co., Ltd.) which are used for cell culture was used for adsorbent. Fig.3-2-2 shows the outline of producing CPB (10). Firstly forming small droplets of a cellulose solution and dropping the droplets into cooling silicon oil (-20 °C) and freeze the droplets. These cellulose solution droplets include water content and the water content is cohered and became small droplets of water content in cellulose solution and grew large water (ice) droplets. After mixing silicon oil for certain time, we added sulfuric acid for regenerating cellulose structure of droplets. After warming the droplet to room temperature, we added epichlorohydrin to the beads for crosslinking cellulose structure.

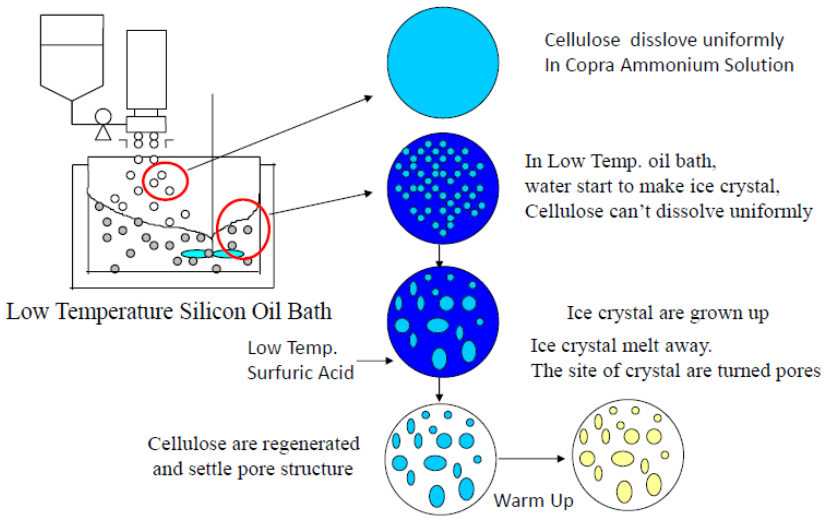

Fig.3-2-2; Outline of Producing Cellulose Porous Beads (CPB)

The structure of CPB is characterized by SEM (Scanning Electron Microscopy) observation and mercury porosimetry.

SEM observation

The CPB sample for SEM observation was prepared by following procedures.

- CPB dispersion solution is displaced ethyl alcohol and t-buthyl alcohol in turn.
- Freeze the CPB dispersion solution in t-buthyl alcohol
- Dry the CPB dispersion solution by evacuation

The surface structure of CPB samples were observed by SEM (S-3000N, Hitachi High Technology Co., Ltd.). The surface observations were conducted by 15keV.

Characterization of pore structure by mercury porosimeter

As mentioned in the chapter 2, gas adsorption is one of the suitable method for characterization of porous materials. But macroporous material characterization is exceptional case. The reason why macroporous characterization is exceptional case is their adsorption capacity and surface area. In general, the gas adsorption is not enhanced in macropore and the surface area is not so large compared with micro- and mesoporous materials because of its large pore width. CPB also can't characterized by N_2 adsorption. Thus mercury porosimeter is taken for characterization.

Autopore 9520 (Shimadu-micrometrics Co., Ltd.) were used for mercury porosimetry. The

initial pressure was settled 6.9 kPa (1 psi) and increased pressure up to 410 MPa (60000 psi). Before starting measurement, the CPB samples were dried under vacuum condition at 473 K. 130 degrees is used as a contact angle of mercury, and 485 dyn/cm is also used as surface tension of mercury for porosity analysis.

Mercury porosimetry, used to investigate macroporosity, is based on the penetration mercury amount, under pressure, into porosity. Pressure is required to force the mercury into the pore structure because it does not wet the pore surface owing to its high contact angle. Washburn suggested the following equation to calculate pore width from mercury intrusion data (11), based on a non- intersection cylindrical pore.

$$w = \frac{4\gamma \cos\theta}{\Delta P} \qquad (3\text{-}2\text{-}1)$$

where w is the pore width (μm), ΔP is the pressure required to force mercury into pore (MPa), γ is the surface tension of mercury, θ is the mercury contact angle toward pore wall.

By mercury porosimerty measurement, we can get the information of mercury pressure and pore volume. Thus, from equation 3-2-1, we can calculate the pore volume (V) which pore width is w. We can get the information of pore size distribution by plotting V against w.

The relationship between pore width and pressure depends on the shape of pore, and this necessitates the selection of a model. Thus, the results obtained the usefulness of the technique as reasonable agreements have been obtained when comparing mercury porosimetry with other models.

T. cruzi adsorption from infectious model blood

Preparation of infectious model blood and column

In order to evaluate *T. cruzi* adsorption rate, we need the infectious blood. But it is too difficult to take this infectious blood. Thus the infectious model blood was prepared for adsorption experiments.

Fig.3-2-3 is the outline of the infectious blood preparation. *T. cruzi* which was cultivated at the culture solution are added to the blood which was taken from mouse. CPD (Citrate Phosphate Dextrose) was used as unti-coagulation medicine. The concentration of *T. cruzi* is $1.0x10^{6}$-$1.0x10^{9}$ counts /ml blood.

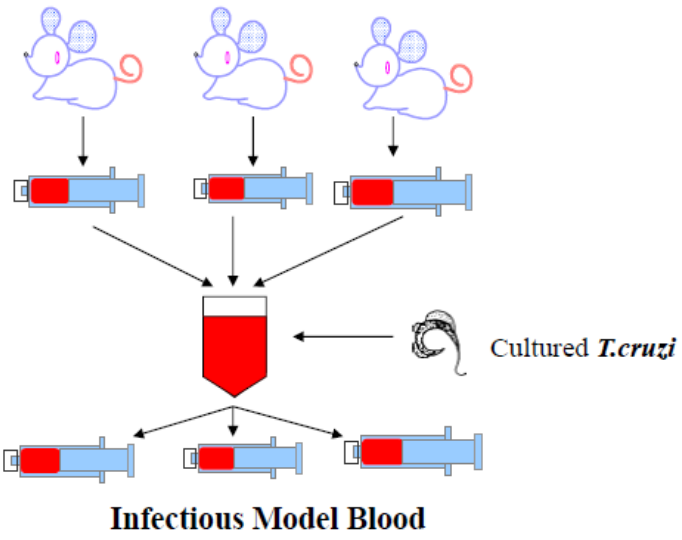

Fig.3-2-3; Outline of Infectious Model Blood Preparation

Fig.3-2-4 shows column (Funakoshi Co., Ltd.) for adsorption experiments. 0.5 ml CPB is fulfilled in this column.

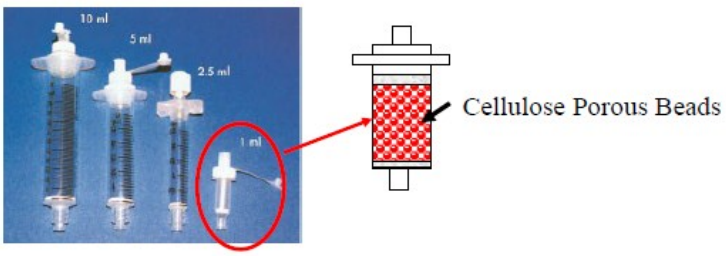

Fig.3-2-4; Column for Flow Adsorption Experiments

T. cruzi adsorption experiments

The adsorption experiments were done by two different way; flow condition and static condition.

Fig.3-2-5-a shows the outline of *T. cruzi* flow adsorption experiments. 8 ml infectious model blood was fulfilled in the syringe (Terumo Co., Ltd.) and set on pump. The flow rate of infectious model blood was set 0.3 ml/min.

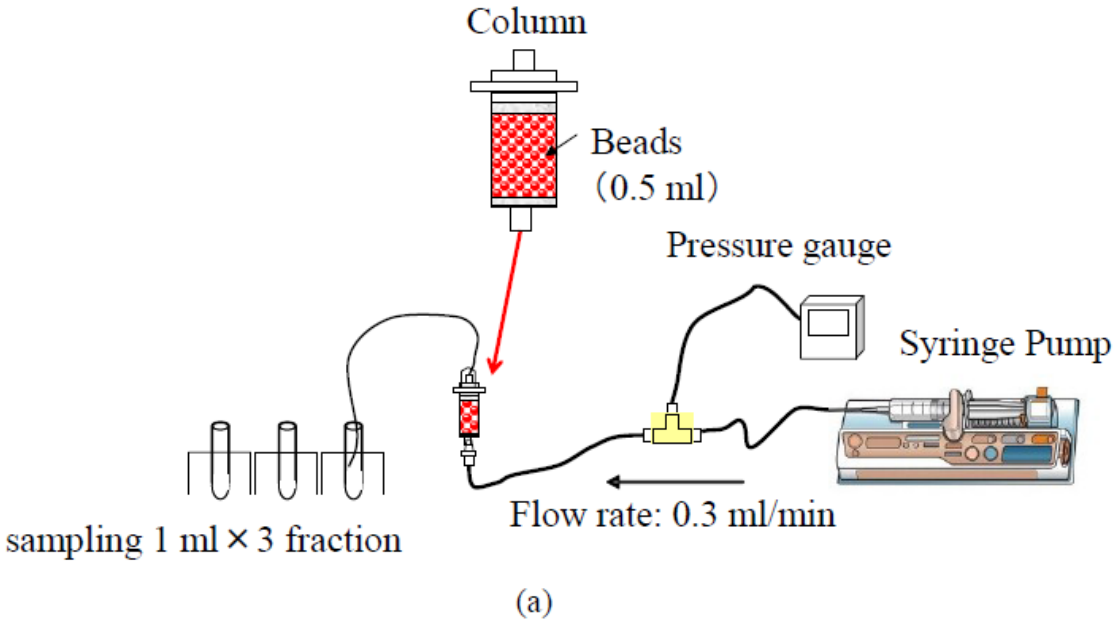

Fig.3-2-5; Outline of *T. cruzi* Adsorption Experiment (a) Flow Adsorption Experiment

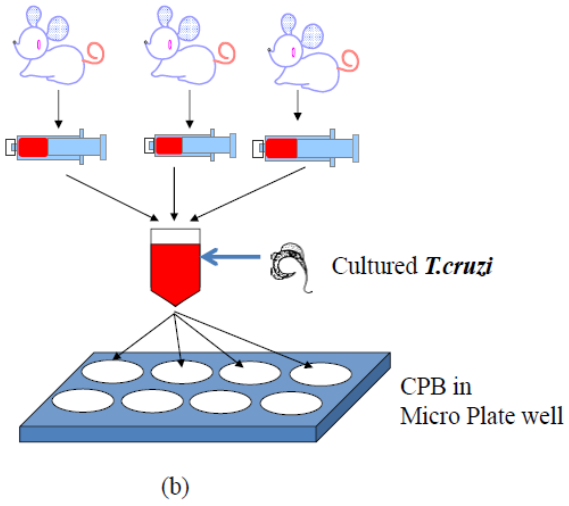

Fig.3-2-5; Outline of *T. cruzi* Adsorption Experiment
(b) Static Adsorption Experiment

The adsorption rate was calculated by pre *T. cruzi* concentration and post *T. cruzi* concentration by following equation.

$$\text{Adsorption rate}\ (\%) = \frac{C_{pre} - C_{post}}{C_{per}} \times 100 \quad (3\text{-}2\text{-}2)$$

where C_{pre} is *T. cruzi* concentration before adsorption, C_{post} is the *T. cruzi* concentration after adsorption.

Fig.3-2-5-b shows outline of another adsorption experiments; static method. One well of micro plate include 0.5 ml CPB with PBS (phosphate buffer solution). After adding 1.5 ml the infectious model blood, the micro plate was incubated in room temperature with 52 rpm shaking. After 1, 4, 8 hour incubation, the concentration of *T. cruzi* in blood was observed. The adsorption rate was calculated by equation 3-2-2.

T. cruzi concentration measurements

Two measurements method; count by microscope method and RT-PCR (Real Time Polymerase Chain Reaction) method, were taken for determination of *T. cruzi* concentration.

Microscope method

100 μL sample blood is taken and diluted 4 times by PBS. After this treatment, 100 μL diluted sample is dropped on slide glass and observe 100-power microscope. The number of *T. cruzi* is counted 4 different windows. The concentration of *T. cruzi* in blood is calculated using following equation.

$$C_{T.cruzi} = Count \times N \times \frac{1\,mL}{100\,\mu L} \qquad (3\text{-}2\text{-}3)$$

where count is the average observed number of *T. cruzi* in 4 windows, N is dilution rate,

RT-PCR (Real Time Polymerase Chain Reaction) method

Microscope method can't detect the adsorption rate over 99 %. Because when CPB adsorbed 99 % of *T. cruzi*, we can't observe any *T. cruzi* by sampling 100 μL blood. In this case, we can't discuss the adsorbed ability over 99 %.

In order to determine *T. cruzi* concentration more precisely, RT-PCR method is used. PCR method is often use for detecting bacteria, virus and so on in blood.

RT-PCR is the method to determine the number of virus and bacteria by amplifying little unique DNA by polymerase chain reaction. Fig.3-2-6 shows the image of polymerase chain

reaction. After we design the primers which have a function to copy the unique DNA configuration, we can start polymerase chain reaction. In this chain reaction process, fluorescent materials are inserted in the DNA chain. By detecting the fluorescence, we can determine the amount of DNA. The chain reaction number of times is proportion to initial DNA amount.

We measure the chain reaction number of times which we can detect the fluorescent and calculate the *T. cruzi* concentration in infectious model blood.

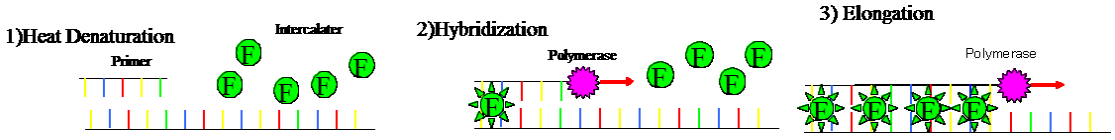

Fig.3-2-6; Image of polymerase chain reaction

By making standard curve, we can determine the concentration of T. cruzi.

The designed primer of *T. cruzi* is as follows.

Accession No	Primer	5'-Base configration-3'
GU075671-	CA001006_F	TGACTACGTGCCGTCTGCTG
	CA001006_R	AAATAGTAGACCCACCATTCGCTGT

The condition of polymerase chain reaction is as follows.

RT-PCR were practiced using Thermal Cycler Dice Real Time System II (Takara Bio Co., Ltd. TP-900)

Contents of reactive solution (25 μL)	
SYBR Premix Ex Ta II	12.5 μL
PCR Forward Primer(10 μM)	1.0 μL
PCR Reverse Primer(10 μM)	1.0 μL
cDNA template	2.0 μL
Dilute to 25 μL by dH_2O	

Reaction condition		
Hold (initial denaturation)	95 ℃	30 sec
2 Step PCR(cycle 40)	95 ℃	5 sec
	60 ℃	30 sec
Dissociation	60 ℃→95 ℃	

In order to determine the *T. cruzi* concentration, we needed standard curve. I made the standard curve as follows.

T. cruzi concentration in infectious model blood; 1.0×10^6 count/mL, was determined by microscope methods.

The dilution system was made as follows by adding PBS in infectious blood.

Dilution times	*T. cruzi* concentration by microscorpe
1	1.0×10^6
5	2.0×10^5
5^2	4.0×10^4
5^3	8.0×10^3
5^4	1.6×10^3
5^5	3.2×10^2
5^6	6.4×10^1
5^7	1.3×10^1

By using these standard infectious model bloods, I can take the information of *T. cruzi* concentration and number of chain reactions (Ct).

Surface observation of CPB after adsorption experiments

In order to analyze the mechanism of *T. cruzi* adsorption on CPB, the surface state of CPB observation was done.

After adsorption experiments, CPB were washed by saline; 5 ml saline was flow in the column in flow experiment, 3 ml saline was added in the well of micro plate in static experiment. After washing, CPB were added in mix solution of 2.0 % paraformaldehyde and 2.5 % glutaraldehyde and incubated at room temperature for one night. After incubation, the treatments of CPB samples are same way as CPB observation.

3-2-3. Results and Discussion

Pore structure of CPB

Fig.3-2-7 shows the relationship between pore width and mercury cumulative intrusion volume. From these relationships, there is large volume increase at 50 μm and 5-10 μm pore width. This increase means that there seems to exist the pores which width is about 5-10 and 50 μm.

Fig.3-2-8 shows the pore size distribution of CPB calculated by mercury porosimetry. This pores size distribution indicates that the pores which width is 5-10 μm and 50 μm are popular on CPB surface. Table 3-2-1 shows the porosities of CPB analyzed in 1-100 μm pore width range. However, I mentioned at SEM observation result, the pores which pore widths are about 50 μm are the interspace of beads from the view point of beads size.

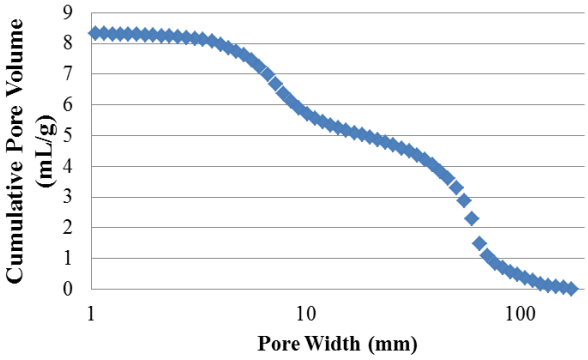

Fig.3-2-7; Relation between Pore width and Mercury Cumulative Intrusion Volume

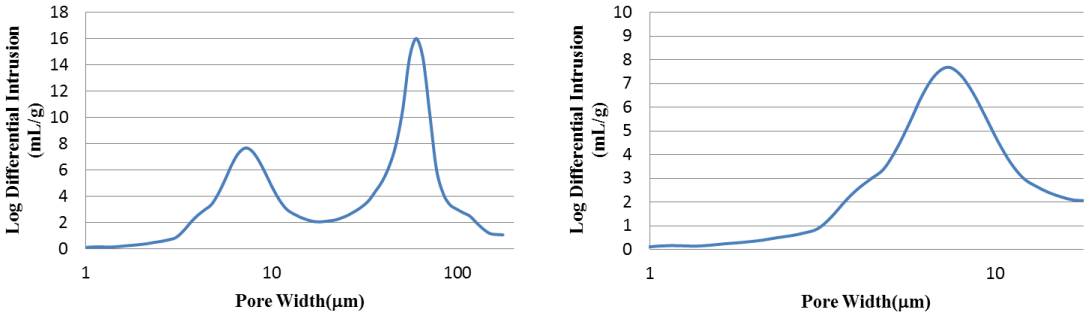

(a) (b)

Fig.3-2-8; Pore Size Distribution of CPB from Mercury Porosimetry
(a)Pore range 1-200 μm, (b) Pore range 1-18 μm

Table3-2-1 shows the pore propertied of CPB by mercury porosimetry.

Table3-2-1; Porosities of CPB by mercury porosimetry (Analysis range; 1-200 μm)

Analysis Range	Pore volume (ml/g)	Surface Area (m^2/g)	Median pore width (μm)
1-100 μm	8.38	3.1	36.7

Fig.3-2-9 shows the SEM observation of surface of CPB. The surface has the pore which pore width is 5-20 μm. However the pores which pores width 50 μm which were measured by mercury porosimetry were not observed by SEM observation. Thus it is natural that the pores which pore width are about 50 μm mean the interspace of beads.

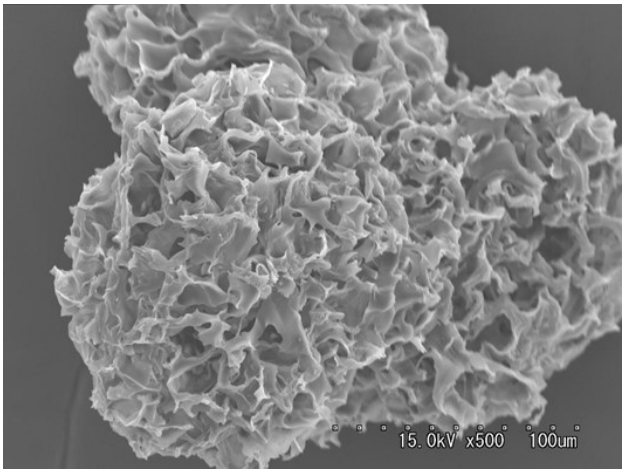

Fig.3-2-9; SEM Observation of CPB

Table3-2-2 shows the porosity of CPB which are calculated from 1 μm-18 μm pore width data. These porosities show the precise value of CPB.

Table3-2-2; Porosities of CPB by mercury porosimetry
(Analysis range; 1-18 μm)

Analysis Range	Pore volume (ml/g)	Surface Area (m^2/g)	Median pore width (μm)
1-18 μm	3.28	2.1	7.2

The most of pores on CPB surface have 5-10 μm. Thus this CPB is suitable for T. cruzi adsorption from blood.

T. cruzi adsorption rate and surface observation of CPB

Table3-2-3 shows the adsorption rate of *T. cruzi* of static adsorption experiments.

Table3-2-3; Results of static adsorption experiments

Incubation time	*T. cruzi* concentration(counts/ml)	Removal rate (%)
Pre adsorption	2.6×10^9	—
1 hour	3.3×10^7	98.7
4 hours	9.2×10^7	96.5
8 hours	3.0×10^7	98.8

Though the pre *T. cruzi* concentration was too high (2.6×10^9 counts/ml), CPB can adsorb and remove 99 % of *T. cruzi* from infected model blood in 1hour. But the adsorption rate of 4 hours and 8 hours later did not increase. These results indicated that the capacities to adsorb *T. cruzi* of CPB are saturated within 1 hour.

Table3-2-4 shows the results of *T. cruzi* adsorption in flow condition experiments. The experiments were done by using two different *T. cruzi* concentration infected blood. The table shows the *T. cruzi* concentration in Pre blood, first 1ml, middle 1ml, and last 1ml fraction, adsorption rate and *T.cruzi* adsorption number on CPB.

Table3-2-4; Results of Adsorption experiments in flow condition

N	Pre *T. cruzi* concentration (counts/ml)	Upper column; *T. cruzi* concentration (count/ml)lower column; removal rate			Adsorbed *T. cruzi* number on CPB (count/gCPB)
		1st fraction	2nd fraction	3rd fraction	
N = 1	2.6×10^9	3.6×10^7	4.4×10^7	3.3×10^7	5.1×10^9
		98.6	98.3	98.7	
N = 2	2.6×10^9	8.6×10^7	1.2×10^7	3.7×10^7	5.1×10^9
		96.7	99.5	98.6	
N = 3	2.6×10^9	8.5×10^7	2.5×10^7	3.8×10^7	5.1×10^9
		96.7	99.0	98.5	
N = 4	1.0×10^6	$< 1.0 \times 10^4$	$< 1.0 \times 10^4$	$< 1.0 \times 10^4$	$> 1 \times 10^6$
		> 99	> 99	> 99	

The N = 1-3 results agreed with the results of static condition adsorption experiments. This agreement indicated that the *T. cruzi* adsorption on CPB occur in short time; just flowing in the column by the 0.3 ml/min low rate. The N = 4 fraction *T. cruzi* concentration shows the lower detection limit of microscope counts. These flowing adsorption experiments show that CPB can adsorb 99 % of *T. cruzi* from infected model blood even from high concentration blood.

In order to understand adsorption capacity more precisely, I analyzed the *T. cruzi* concentration by RT-PCR. Table3-2-5 shows the result of RT-PCR of N=4 infected blood sample.

Table3-2-5; Results of Adsorption experiments in flow condition

sample	Ct value	Log(T. cruzi)	*T. cruzi* concentration(counts/mL)	Adsorption rate(%)
Pre adsorption	21.74	6.00	1.0×10^6	-
Fraction 1	28.01	4.28	1.9×10^4	98.1
Fraction 2	27.90	4.30	2.0×10^4	98.0
Fraction 3	26.98	4.55	3.5×10^4	96.5

where Ct value means polymerase chain reaction cycle number.

This cycle time is proportion to *T. cruzi* concentration. Fig.3-2-10 shows the relation cycle number and fluorescence of 5 different concentration standard infected bloods.

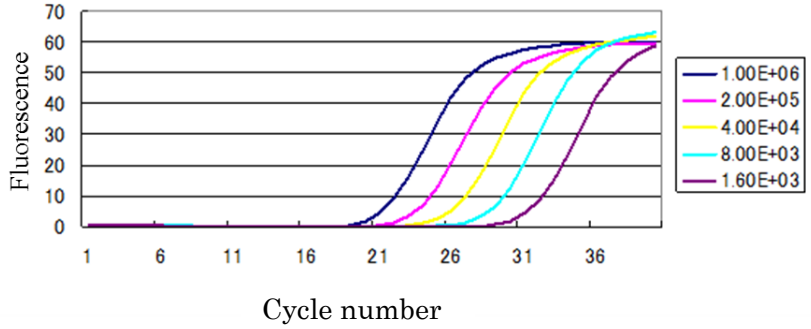

Fig.3-2-10; Relation between cycle time and fluorescence of *T. cruzi*

From RT-PCR results, we took the following relationship between cycle number and *T. cruzi* concentration.

$$Ct = -3.689 \times \mathrm{Log}(T.\ cruzi\ \text{concentration}) + 43.794$$

Thus I calculated the sample *T. cruzi* concentration by this equation. RT-PCR results also agreed with the result of microscope results. CPB can adsorb and remove *T. cruzi* from infected model blood.

SEM observation of CPB after adsorption experiments

At previous section, CPB can adsorb *T. cruzi* from infectious model blood. But there was no information of adsorption mechanism of *T. cruzi* on CPB surface. In order to analyze *T. cruzi* adsorbed state on CPB surface and estimated the mechanism, SEM observation of post adsorption experiments were done.

Fig.3-2-11-a-d shows the SEM observation of CPB.

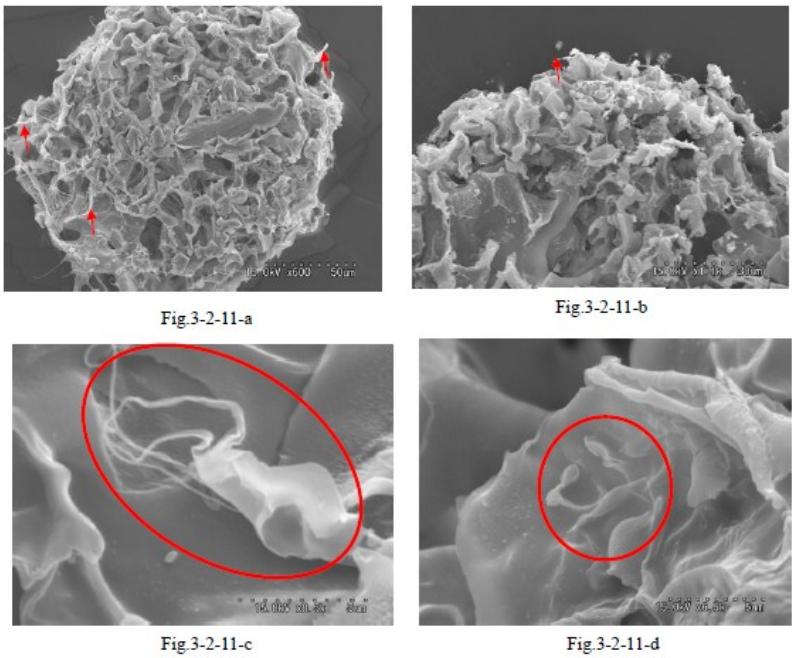

Fig.3-2-11-a

Fig.3-2-11-b

Fig.3-2-11-c

Fig.3-2-11-d

Fig.3-2-11; Post adsorption experiment CPS surface

Fig.3-2-11-a & b shows the whole surface of CPB. Even low magnification (600-powers), there were many fibrous materials on the surface of CPB; red arrows in Fig.3-2-11-a & b. It can be flagellums of *T. cruzi*. Fig.3-2-11-c & d shows the high magnification of CPB surface. *T. cruzi* are adsorbed on the flat surface of CPB and removed; red circle in Fig.3-2-11-c. From these SEM observations, *T. cruzi* were adsorbed on the surface of CPB. The adsorbed states of *T. cruzi* on CPB indicate that *T. cruzi* did not adsorbed in macropore but on the flat surface of CPB. Initially, I had the hypothesis that *T. cruzi* adsorbed on the macropores, but this hypothesis is not collect because *T. cruzi* adsorbed on the flat surface of CPB. From Fig.3-2-11-c & d, they indicated that there is another mechanism to *T. cruzi* adsorption.

I tried to estimate the mechanism of *T. cruzi* adsorption on CPB surface from some other results of experiments. *T. cruzi* did not adsorb just on cellulose surface because another cellulose beads (Viscobal, Rengo co., Ltd.) can't be adsorbed *T. cruzi*.

There is a clue in the unique chemical structure of CPB. Fig.3-2-12 shows the image of chemical structure. Cellulose of CPB is cross-linked by epichlorohydrin for reinforcement of structure after regenerated by sulfuric acid. In this reinforcement process, not all epichlorohydrin crosslink cellulose completely. There are some cases that just one side of epichlorohydrin react cellulose; red circle in Fig.3-2-12. When epichlorohydrin react hydroxyl group, the structure is resemble to the structure of Sialic acid; red circle in Fig.3-2-13.

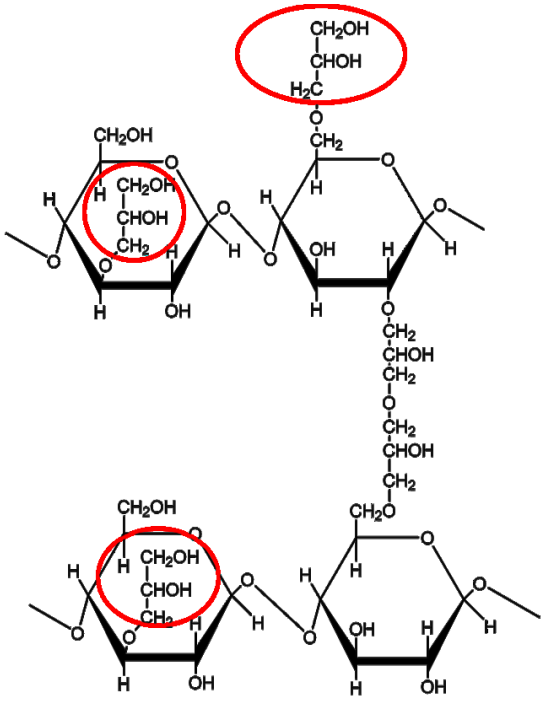

Fig.3-2-12; Chemical structure of CPB

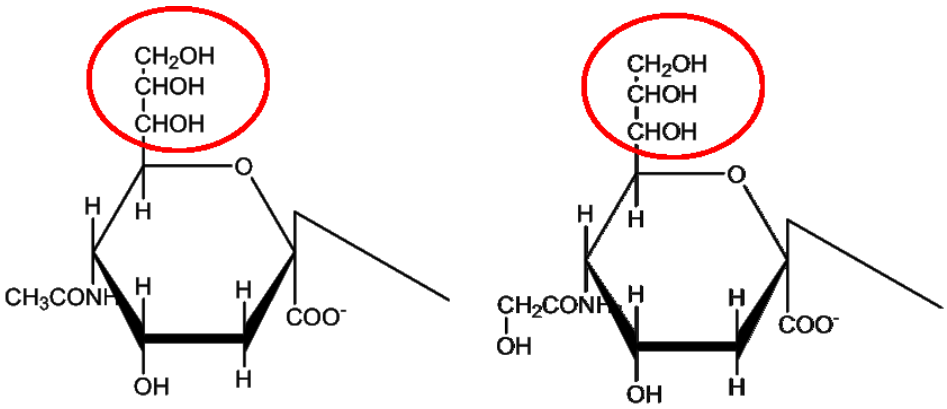

Fig.3-2-13; Chemical structure of Sialic acid

On the other hand, Yoshida et al. (12) declared the mechanism of *T. cruzi* invention in human cells. According to Yoshida's analysis, *T. cruzi* can recognize the only human cell by certain enzyme; trans-sialidase on *T. cruzi* cell surface. Trans-sialidase on T. cruzi cell surface recognizes the mucin like glycoprotein on human cell and invades in it. The most of mucin like

glycoprotein on human surface is sialic acid. Thus, *T. cruzi* can invade human cell uniquely by the recognition of sialic acid of human cell surface. Schenkmann also reported that *T. cruzi* can't invade the cell which sialic acid was masked (13).

These results indicated that there is a possibility that sialic acid like chemical structure of CPB surface contributes to T. cruzi adsorption.

But we have to further examination to determine the sialic acid like chemical structure is cause of *T. cruzi* adsorption on CPB surface.

References

Chapter 3-2

(1) W.M. Lee, New Eng. J. Med., 337, 1997, 1733, http://dx.doi: 10.1056/NEJM/99712113372406.

(2) J.L. Dienstag, Hepatology, 26, 1997, 66S, http://dx.doi: 10.1002/hep.510260712.

(3) S. Wendel, Blood Safty and surveillance, Medical Dekker Inc. New York, 2003, 355.

(4) S. Seidl, Transfusion, 30, 1990, 355, http://dx.doi: 10.1046/j.1537-2995.1990.30991048779.x.

(5) S. Wendel, J.A.J. Barbara, F. Frcp, Global perspectives in transfusion medicine, 2006, aabb Press, Bethesda Maryland.

(6) L.A. Beltz and F. Kierszenbaum, Immunology, 60, 1987, 309.

(7) Z. Brener, Adv. Parasitol, 18, 1980, 247, http://dx.doi: 10.1016/S0065-308x(08)60401-7.

(8) L. Hudson, Ann. Soc. Belge Med. Trop., 65, 1985, 71.

(9) F. Kierszenbaum, J.Parasitol, 72, 1986, 201, http://dx.doi: 10.2307/3281592.

(10) J. Hamada, Y. Ushio, K. Kazekawa, T. Tsukahara, N. Hoshino and H. Iwata, Am. J. Neuroradiol, 17, 1996, 1895.

(11) S.J. Gregg and K.S.W. Sing, Adsorption, Surface Area and Porosity, London, Academic Press, 1967

(12) N. Yoshida, World class parasites; Volume 7 American Trypanosoma, Kluwer Academic publishers, London, 69.

(13) S. Schenkman, D. Eichinger, M.E.A. Pereira and V. Nussenzweig, Ammu. Rev. Microbiol, 48 1994,499, http://dx.doi: 10.1146/annurev.mi.48.100194.002435.

4. Summary

In this thesis, I examined the structure of porous materials, gas adsorption mechanism and their use for medical treatment.

The adsorption mechanism on mesopores was analyzed and the cause of adsorption hysteresis was investigated. The adsorption isotherms of various gases (N_2, O_2, Ar, and He) for various uniform mesoporous materials (Pore width; 2.5 nm-8.3 nm) were examined. The adsorption isotherms of mesopore which pore width is below 3.4 nm did not have adsorption hysteresis. Saam-Cole approach analysis indicated that there is difference of layer thickness (l_c- l_e) between adsorption form change from multi-layer to condensation (l_c) in adsorption process and condensation to multi-layer (l_e) in desorption process. When l_c- l_e become lower certain value (N_2: 0.09 nm, O_2: 0.10 nm, Ar: 0.10 nm, He: 0.08 nm), the adsorption hysteresis disappear. Because when (l_c- l_e) become lower certain value, (l_c- l_e) would be veiled by the atomic level ambiguity of adsorbed layer thickness.

Secondly, the relationship between structure of activated carbon and cytokine adsorption mechanism was declared. There are many cytokines in human immune systems. Cytokines have various character; molecular weight, electric character. Thus, it is difficult to remove various cytokines from blood or plasma simultaneously.

I focused on the nonspecific adsorption ability of activated carbon. The activated carbon (AC) which is used for extracorporeal column (Hemosoba Asahi kasei medical Co., Ltd.) was examined for cytokines and HMGB1 adsorption experiments. The AC has micropore and 5-20nm pore width mesopores from N_2 adsorption.

The 18 cytokines which molecular weight is 8-70 kDa and HMGB1 adsorption ability by ACs were examined. ACs can adsorb all 18 cytokines and HMGB1. However the removal rate is depended on their molecular weight. The larger the molecule of cytokine is, the lower the adsorbed rate become. The detail analysis of 18 cytokines and HMGB1 adsorption isotherms give us the information of adsorption mechanism. The adsorption mechanisms are changed by cytokines molecular weight for ACs as follows.

- 8-10 kDa molecular weight cytokine; adsorbed in mesopore in low concentration
- 10-20 kDa molecular weight cytokine; adsorbed in mesopore and after saturated, adsorbed on extra surface area.
- 20-30 kDa molecular weight cytokine and HMGB1; part of cytokines and HMGB1 can adsorbed in mesopore at low concentration, but most of them adsorbed on extra surface of ACs.
- Over 30 kDa molecular weight cytokines; can't adsorbed in mesopore, the adsorbed amount at low concentration is too small, at high concentration, the adsorbed amount increase.

These mechanisms are different in each porosity of ACs. This mechanism will be an important data for designing the more suitable pore structure of adsorbent for cytokine adsorption.

In this thesis, the evaluation system for many cytokines adsorption ability by preparing inflammatory model plasma was established.

Thirdly, the materials for adsorbing parasite; *T.cruzi* which is the pathogens of Chagas

disease, were examined. *T.cruzi* adsorption ability by macropore was investigated. Because the *T.cruzi* size; 1-5 μm is suitable to macropore. The adsorption rate of *T.cruzi* from infected blood was over 99 %. Even the concentration of *T.cruzi* is high blood; CPB can adsorb over 99 % of *T. cruzi* from whole blood.

By analyzing the state of adsorption on CPB, *T. cruzi* did not adsorb by macropore effect but adsorbed by certain chemical interactions. The mechanism of *T.cruzi* adsorption was estimated the unique chemical structure of CPB surface. The surface structure of CPB is resembled to the sialic acid which is the key structure when *T. cruzi* recognize and invade human cell. Thus, *T.cruzi* removal mechanism of CPB is estimated that *T. cruzi* recognize the CPB surface as human cell surface and adsorbed.

However this is just the estimation from indirect evidence, further examination will be necessary to determine the mechanism perfectly.

Until today, there has been little research of adsorbent for medical use. Today the technology for controlling porosities and biocompatibilities of carbon and other material are developed. The adsorbent research for medical use should be examined. The adsorption treatments for sepsis and infectious disease have potential to be a good treatment because adsorption treatments don’t have side effects like medicines.

Acknowledgment

I would like to express my sincere thanks to those who have made the completion of this thesis possible.

My supervisor Prof. Hirofumi Kanoh for his precious advice and instrumentality. Thank you for giving the opportunity to complete my PhD studies in your group.

Prof. Katumi Kaneko for giving the theme of master thesis and chance to enter the graduate school of Chiba University, Professor of Shinshu University.

Dr. Norihiko Setoyama, for his valuable advice in Chiba University, Toyota Central Research.

Prof. Yoko Hanzawa for her kind advice to complete master thesis in Chiba University, Professor of Chiba Institute of Technology.

Dr. Taku Iiyama for his kind and valuable advice for many kinds of experiments in Chiba University, Associate Professor of Shinshu University.

Dr. Sachiyo Miura for giving us the chance to evaluate removal rate of *T. cruzi,* Former associate Professor of Keio University.

Dr. Yoshihiro Hatanaka for giving the chance to enter doctor course and precious support to complete this thesis, Leader of Medical Material Laboratory in Oita Asahi Kasei Medical Co. LTD.

Mr. Kentaro Kiriyama for his valuable support of adsorption experiments, Asahi Kasei Medical Co. LTD.

All other member of Medical Material Laboratory of Asahi Kasei Medical for their supports.

Past colleagues at Chiba University for creating homely atmosphere and inspiring,

motivating. Especially, Ms. Kyoko Nishigaya, Dr. Jin Miyawaki.

Finally, my wife and son for their support and encouragement, my parents and sister for giving me a chance to enter university and supports.

January 5th, 2015

Satoru INOUE

List of publications

1) S. Inoue, Y. Hanzawa, and K. Kaneko; Prediction of Hysteresis Disappearance In the Adsorption Isotherms of N_2 on Regular Mesoporous Silica; Langmuir, 14, 3079, (1998), http://dx.doi:10.1021/la971256u.

2) S. Inoue, K. Kiriyama, Y. Hatanaka, and H. Kanoh, Adsorption Properties of an Activated Carbon for 18 Cytokines and HMGB1 from Inflammatory Model Plasma; Colloid and Surfaces B: Biointerfaces, 126, 58, (2015), http://dx.doi:10.1016/j.colsurfb.2014.12.015.

3) S. Inoue, N. Ichikuni, T. Suzuki, T. Uematsu, and K. Kaneko; Capillary Condensation of N_2 on Multiwall Carbon Nanotubes; J. Physical Chemistry B, 102, 4689, (1998) , http://dx.doi:10.1021/jp973319n.